PAPER • OPEN ACCESS

NV$^-$–N$^+$ pair centre in 1b diamond

View the article online for updates and enhancements.

New Journal of Physics

The open access journal at the forefront of physics

PAPER

CrossMark

NV⁻–N⁺ pair centre in 1b diamond

Neil B Manson[1] , Morgan Hedges[1] , Michael S J Barson[1] , Rose Ahlefeldt[1] , Marcus W Doherty[1] , Hiroshi Abe[2] , Takeshi Ohshima[2] and Matthew J Sellars[1]

[1]   Laser Physics Centre, Research School of Physics and Engineering, Australian National University, Canberra, A.C.T. 2601, Australia
[2]   National Institutes for Quantum and Radiological Science and Technology, 1233 Watanuki, Takasaki, Gunma 370-1292, Japan

E-mail: Neil.Manson@anu.edu.au

Keywords: nitrogen-vacancy, optical spectroscopy, Stark effect, spin polarisation
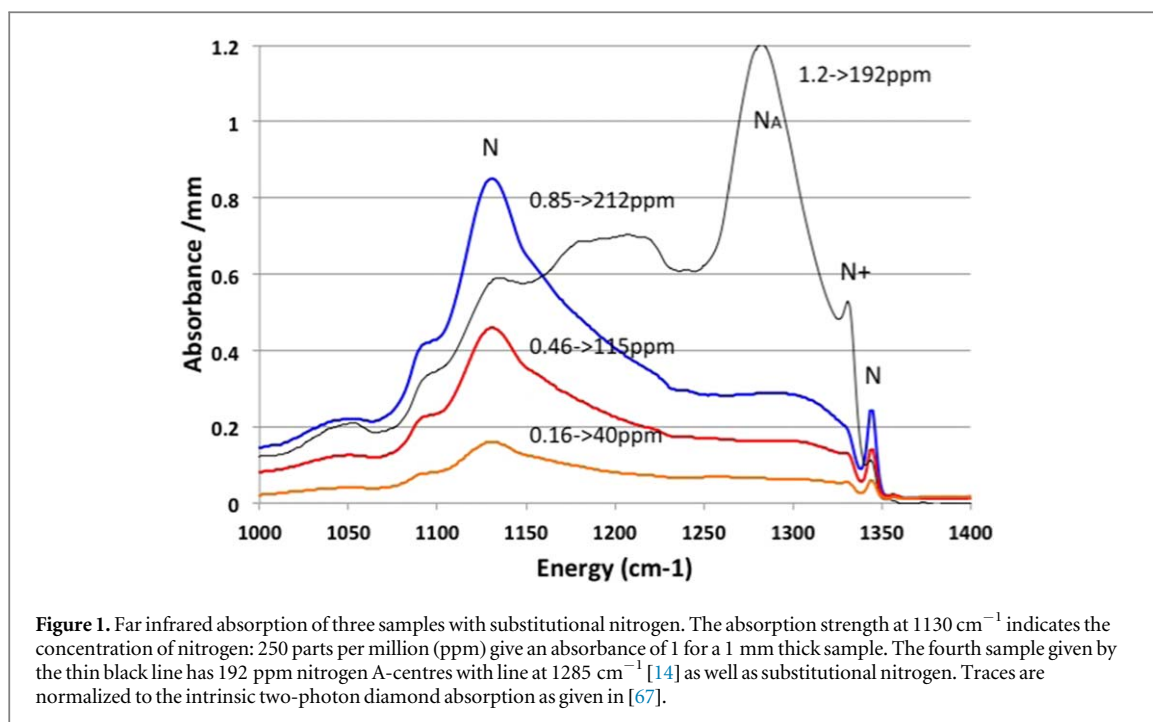
Abstract

With the creation of nitrogen (NV) in 1b diamond it is common to find that the absorption and emission is predominantly of negatively charged NV centres. This occurs because electrons tunnel from the substitutional nitrogen atoms to NV to form $NV^-–N^+$ pairs. There can be a small percentage of neutral charge NV^0 centres and a linear increase of this percentage can be obtained with optical intensity. Subsequent to excitation it is found that the line width of the NV^- zero-phonon has been altered. The alteration arises from a change of the distribution of N^+ ions and a modification of the average electric field at the NV^- sites. The consequence is a change to the Stark shifts and splittings giving the change of the zero-phonon line (ZPL) width. Exciting the NV^- centres enhances the density of close N^+ ions and there is a broadening of the ZPL. Alternatively exciting and ionizing N^0 in the lattice results in more distant distribution of N^+ ions and a narrowing of the ZPL. The competition between NV^- and N^0 excitation results in a significant dependence on excitation wavelength and there is also a dependence on the concentration of the NV^- and N^0 in the samples. The present investigation involves extensive use of low temperature optical spectroscopy to monitor changes to the absorption and emission spectra particularly the widths of the ZPL. The studies lead to a good understanding of the properties of the $NV^-–N^+$ pairs in diamond. There is a critical dependence on pair separation. When the $NV^-–N^+$ pair separation is large the properties are as for single sites and a high degree of optically induced spin polarization is attainable. When the separation decreases the emission is reduced, the lifetime shortened and the spin polarization downgraded. With separations of $<12\,A^0$ there is even no emission. The deterioration occurs as a consequence of electron tunneling in the excited state from NV^- to N^+ and an optical cycle that involves NV^0. The number of pairs with the smaller separations and poorer properties will increase with the number of nitrogen impurities and it follows that the degree of spin polarization that can be achieved for an ensemble of NV^- in 1b diamond will be determined and limited by the concentration of single substitutional nitrogen. The information will be invaluable for obtaining optimal conditions when ensembles of NV^- are required. As well as extensive measurements of the NV^- optical ZPL observations of Stark effects associated with the infrared line at 1042 nm and the optically detected magnetic resonance at 2.87 GHz are also reported.

1. Introduction

A vacancy adjacent to a substitutional nitrogen (NV) in diamond can be detected at the single site level. The negatively charged centre NV^- has a spin ($S = 1$) ground state that can be optically pumped into one spin projection with near 100% efficiency and the spin projection read optically, all under ambient conditions. These capabilities have lead to a phenomenal array of single NV^- applications in life sciences, magnetic sensing, quantum information processing and nano-detection. (see reviews: [1–4]). There are also applications that utilize ensembles of NV^- centres. These includes detection of magnetic fields with the possibility over wide areas [5–8] and often for materials with biological [9, 10] or geological interest [11, 12]. In the case of these latter

Figure 1. Far infrared absorption of three samples with substitutional nitrogen. The absorption strength at 1130 cm^{-1} indicates the concentration of nitrogen: 250 parts per million (ppm) give an absorbance of 1 for a 1 mm thick sample. The fourth sample given by the thin black line has 192 ppm nitrogen A-centres with line at 1285 cm^{-1} [14] as well as substitutional nitrogen. Traces are normalized to the intrinsic two-photon diamond absorption as given in [67].

ensemble applications it is desirable that the NV$^-$ centres maintain the properties of the single centres. However when ensembles are used the novel properties are degraded but to what extent has not been quantified or explained. The aim of this paper is to investigate the optical properties of nitrogen vacancy centres in diamond and focus on how and to what extent the properties of NV$^-$ centres are corrupted and what limits their properties.

The negative charge state requires an electron from a donor in the diamond lattice, usually from a substitutional nitrogen and in this case forms an NV$^-$–N$^+$ pair. The donor is essential but if well separated from the NV$^-$ it has little influence on the properties of the NV$^-$ centre and this is the preferred situation for using a single NV$^-$ centre for applications. With NV$^-$ in 1b diamond there is a density of substitutional nitrogen atoms and for a given NV centre any one of the substitutional nitrogen atoms can provide the electron to form the NV$^-$–N$^+$ pair. In this work it is shown that the properties of the NV$^-$–N$^+$ pair centre vary with separation of the pair and it is the average properties that are observed, measured and utilized in any application. Optical excitation that is used to initialize and measure the centre can also change the NV$^-$–N$^+$ separation and in the process modify the properties. The focus of this paper is to explain how this occurs and give details of the dependence on nitrogen concentration and excitation wavelength. The investigation relies on low temperature optical spectroscopy and an overview of optical characteristics and spectra of the NV system is included by way of an introduction.

2. Experimental details

2.1. Samples

In 1b diamond nitrogen atoms substitute for carbon atoms at lattice sites. Such single substitutional nitrogen can act as an electron donor and the donor enables the creation of the negatively charged NV centre that is of primary interest in this study. 1b is the normal diamond type for synthetic diamond when prepared using high temperature and high pressure and nitrogen concentrations are frequently reported to be of order of 100's parts per million (ppm). Such crystals are available commercially, for example, from Element-6 or Sumitomo. This study focuses on three such samples available from previous studies [13]. From the strength of the infrared absorption at 1130 cm^{-1} [14] the three samples were found to have 212, 115 and 40 ppm single-substitutional nitrogen impurities (figure 1). A fourth sample was also investigated but was not strictly 1b diamond as it contained 192 ppm nitrogen incorporated as nitrogen pairs (A-centre) in addition to some substitutional nitrogen (1a diamonds has A-centres only). From observation of variation in color it is obvious that the samples exhibit significant inhomogeneities and the nitrogen concentrations are only accurate to 20%. All samples have cross section of a few mm's and are slightly more than mm thick. Specific details as well as information of other samples are given later.

The nitrogen-vacancy centre in diamond is formed with irradiation that create vacancies (here 2 MeV electrons at 1×10^{17} to 1×10^{18} cm^{-2} using procedures similar to that in reference [15]) followed by annealing. The annealing at temperatures >700 °C cause the vacancies to become mobile and be trapped at nitrogen sites to form the nitrogen-vacancy pairs. Each pair is aligned along a $\langle 111 \rangle$ direction to give a centre with trigonal symmetry (C_{3V}). The centre can occur in the neutral charge state NV^0, negative charge state NV$^-$ or positive charge state NV$^+$ [16]. The positive charge state is not optically active and is unlikely to occur in 1b diamond with the density of donors. The neutral NV^0 and negative NV$^-$ charge state centres have prominent optical transitions with zero-phonon lines (ZPL) at 575 nm (2.156 eV, 17389 cm^{-1}) and at 637 nm (1.945 eV, 15687 cm^{-1}), respectively. The concentration of NV centres can be determined from the strength of the low temperature absorption of the ZPL [17] and in the case of NV$^-$ the concentrations for the samples studied are 0.5 ppm, 0.8 ppm and 0.2 ppm (each $\pm 20\%$) for the samples with 212 ppm, 115 ppm and 40 ppm nitrogen, respectively. The initial part of the study focuses on the sample with 115 ppm nitrogen (and 0.8 ppm NV$^-$). This is followed by the study of two other samples, one with the higher nitrogen concentration of 212 ppm nitrogen (and 0.5 ppm NV$^-$) and one with lower nitrogen concentration of 40 ppm (and 0.2 ppm NV$^-$).

2.2. Equipment

The experiments involved low temperature optical spectroscopy with the samples within a cryostat at temperatures between 300 and 4 K. The absorption and emission spectra were analyzed using a 1/3 meter monochromator with a possible resolution of 0.12 nm. In the visible the detection involved a GaAs-photomultiplier with response from 400 to 900 nm and in the infra-red by a liquid-N$_2$ cooled Ge detector with response from 800 to 2000 nm. Emission is in arbitrary units given by the output of the detector not corrected (with one exception) for spectral response. Absorption response was obtained from the measurement of transmission of white light from a current-stabilized tungsten light source. The lasers available were a 5 Watt Ar$^+$ ion laser with wavelengths 514, 501, 496, 488, 476 and 458 nm, two tunable dye lasers with wavelengths fixed or swept within the range 670–570 nm and intensities from 10 to 500 mW depending on wavelength, and fixed frequency lasers at 532 nm (to 5 W) and 445 nm (to 400 mW).

The sample inhomogeneities give rise to inconsistencies when focusing to small spot sizes and so no focusing was used and excitation was over a 2 mm diameter spot. It follows that it is convenient to give intensities over mm^2. For example a 3 mW beam has an energy density of order of 1 mW mm^{-2}. It is found that laser excitation can modify the properties of the diamond samples but at the wavelengths generally used of 532 or 620 nm this does not occur for intensities <1 mW mm^{-2} and such intensities are termed 'low intensity'. These intensities are used when sample modifications are to be avoided. Higher intensities are used in other cases and will be given in mW mm^{-2}. Population occurs in the excited and metastable states but intensities are never sufficiently for these populations to be significant fraction of total population and $<1\%$.

3. Properties of NV centres
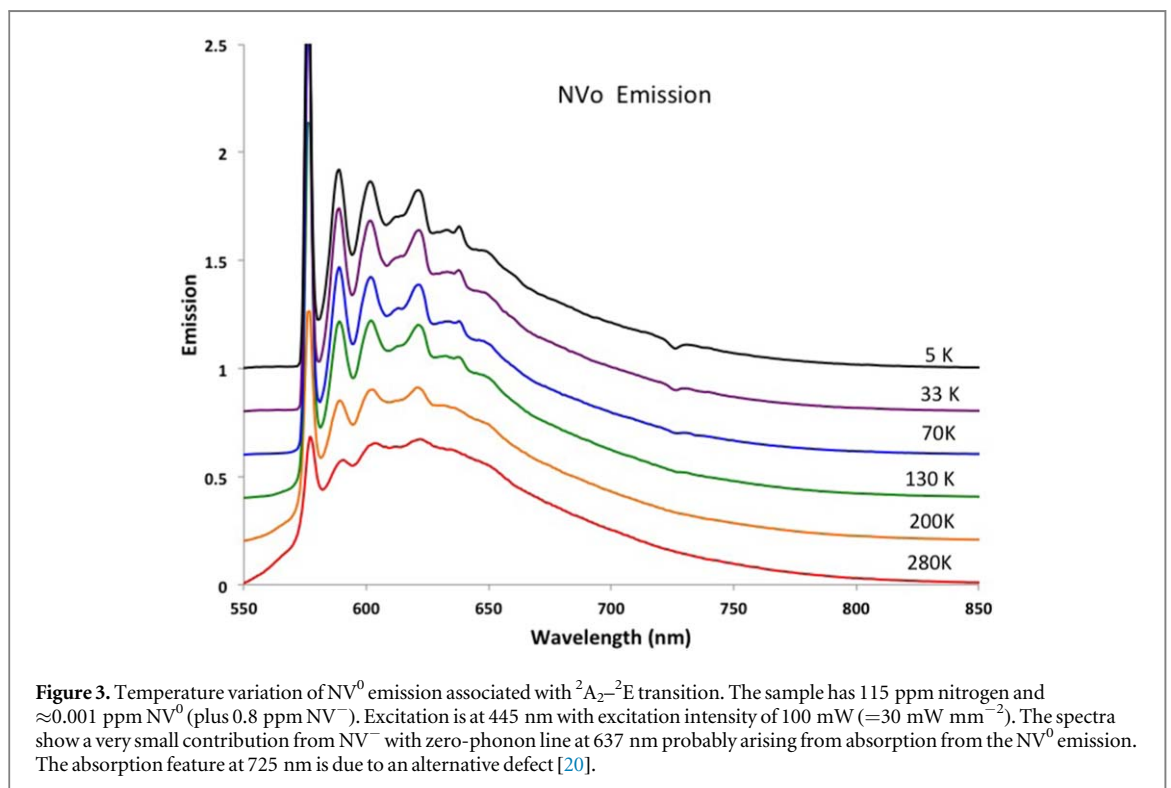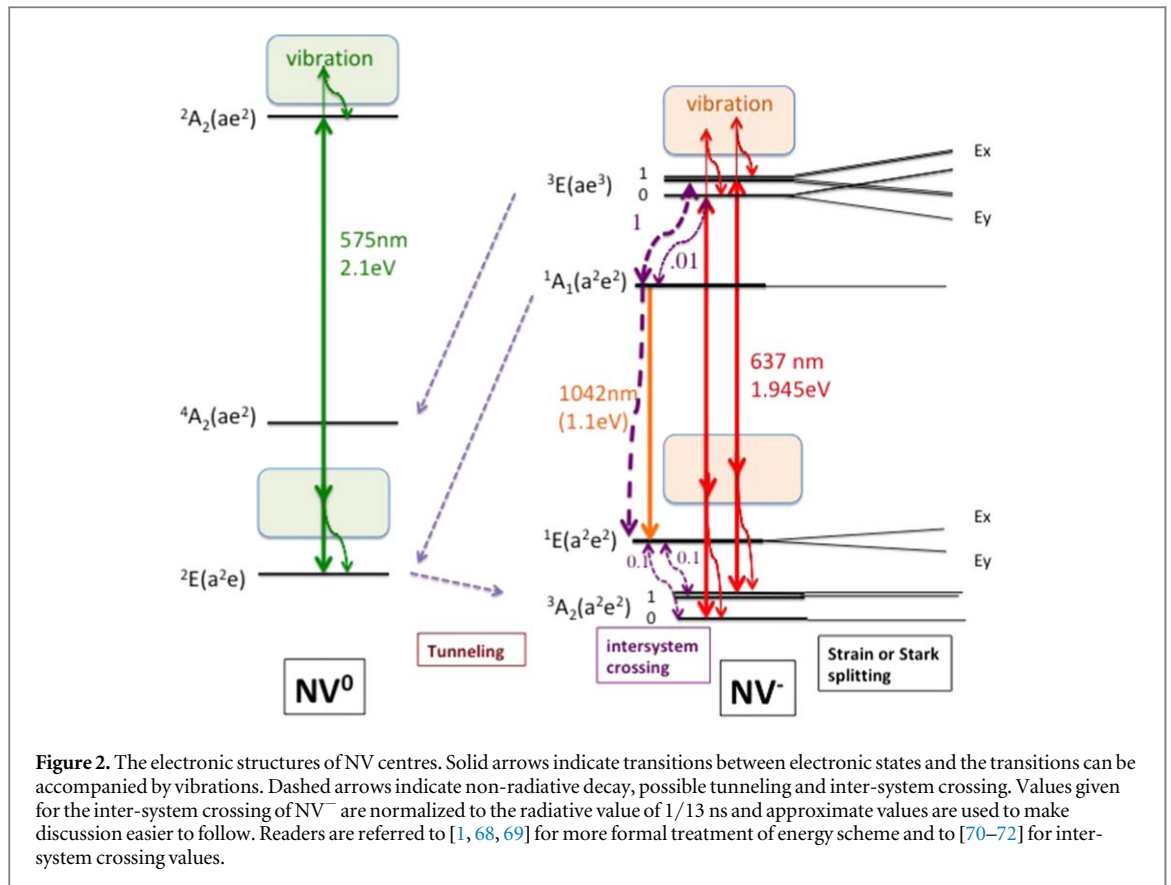
3.1. Electronic structure

The NV$^-$ and NV^0 centres have been studied extensively and the electronic structures are well established [1]. To assist discussion simplified schematics of the structures are given in figure 2.

3.2. NV^0 centre

The neutral centre, NV^0 has the ZPL at 575 nm and the optical transition has been shown to be between a ^{2}E ground state and ^{2}A$_2$ excited state [18]. An electron spin resonance signal has also been detected and attributed to an intermediate ^{4}A$_2$ state [19]. Modeling of the vacancy centres in diamond is described by molecular orbitals formed from the dangling bonds of the carbon atoms associated with the vacancy in addition to orbits of any adjacent impurities. In the case of the nitrogen-vacancy there is a non-degenerate a$_1$ orbit in the valence band that is generally ignored. In the gap between valence and conduction bands there is a non-degenerate a$_1$ and a degenerate e state (of A$_1$ and E symmetry, respectively in C$_{3V}$) and it is the occupation of these one-electron states that give the electronic levels. For NV^0 there are three (neglecting the one in the valence band) electrons giving the ^{2}E(a$_1^2$e) ground state, the ^{2}A$_2$(a$_1$e^2) excited state and the intermediate ^{4}A$_2$(a$_1$e^2) state. The optical transition has a Huang–Rys factor of $S = 3.3$ [20] giving only 3.7% ($e^{-S} = 0.037$) of the oscillator strength in the ZPL and most of strength in the vibronic band. The ^{2}E–^{2}A$_2$ absorption stretches from 575 to 400 nm and emission from 575 to 700 nm as shown in figure 3.

3.3. NV$^-$ centre

In the case of the negatively charged NV$^-$ centre the transition at 637 nm involves a transition between an orbital A$_2$ ground state and excited E orbital doublet [21]. Both states involve four electrons and are spin triplets, ^{3}A$_2$(a$_1^2$e^2)

Figure 2. The electronic structures of NV centres. Solid arrows indicate transitions between electronic states and the transitions can be accompanied by vibrations. Dashed arrows indicate non-radiative decay, possible tunneling and inter-system crossing. Values given for the inter-system crossing of NV⁻ are normalized to the radiative value of 1/13 ns and approximate values are used to make discussion easier to follow. Readers are referred to [1, 68, 69] for more formal treatment of energy scheme and to [70–72] for inter-system crossing values.

Figure 3. Temperature variation of NV^0 emission associated with $^2A_2$–^2E transition. The sample has 115 ppm nitrogen and ≈ 0.001 ppm NV^0 (plus 0.8 ppm NV^-). Excitation is at 445 nm with excitation intensity of 100 mW (=30 mW mm^{-2}). The spectra show a very small contribution from NV^- with zero-phonon line at 637 nm probably arising from absorption from the NV^0 emission. The absorption feature at 725 nm is due to an alternative defect [20].

and $^3E(a_1e^3)$ as shown in figure 2. The optical transitions involve transitions between like-spins and the three spin projections for $m_s = 0$, $m_s = +1$ and $m_s = -1$ have equal strength. The transition has a Huang–Rys factor of $S = 3.65$ [21] which implies the ZPL involves only 2.6% ($e^{-S} = 0.026$) of the overall transition strength and most of the signal is associated with the accompanying vibrational sidebands. The bands in absorption and emission are shown in figures 4 and 5, respectively. As shown in the electronic structure in figure 2 there is inter-system crossing
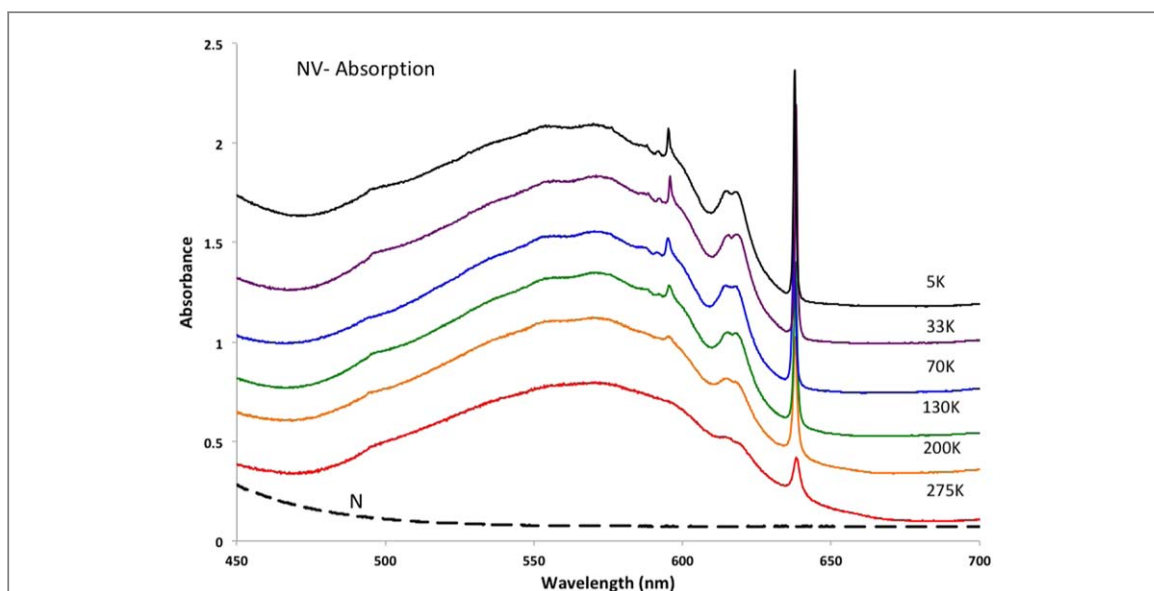
Figure 4. The $^3A_2$–^3E absorption of NV^- for various temperatures between 275 and 5 K for a 1.63 mm thick sample with an NV^- concentration of 0.8 ppm and N^0 concentration of 115 ppm. Absorption is obtained from the transmission of light from a tungsten light source. The dashed line is the variation of absorption of singly-substitutional nitrogen obtained from a separate sample with equivalent nitrogen concentration. The impurities that give the features at 595 and 494 nm commonly occur in irradiated HPHT diamonds but not associated with NV^- [20].
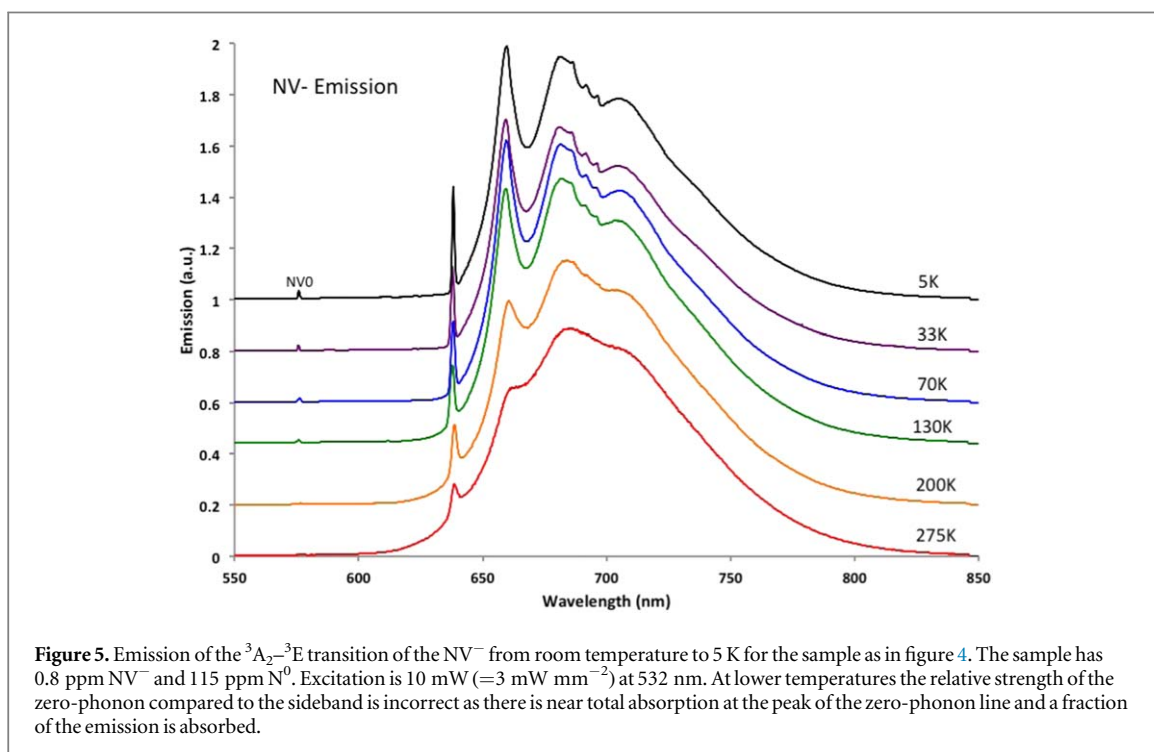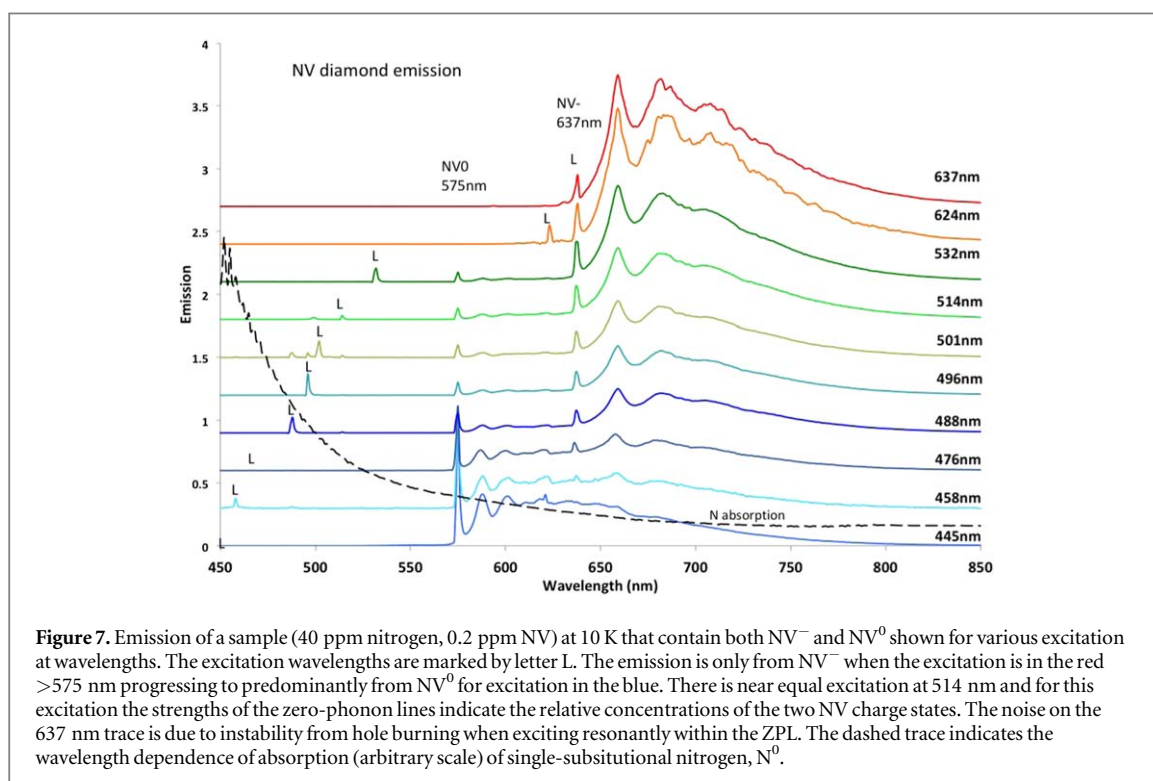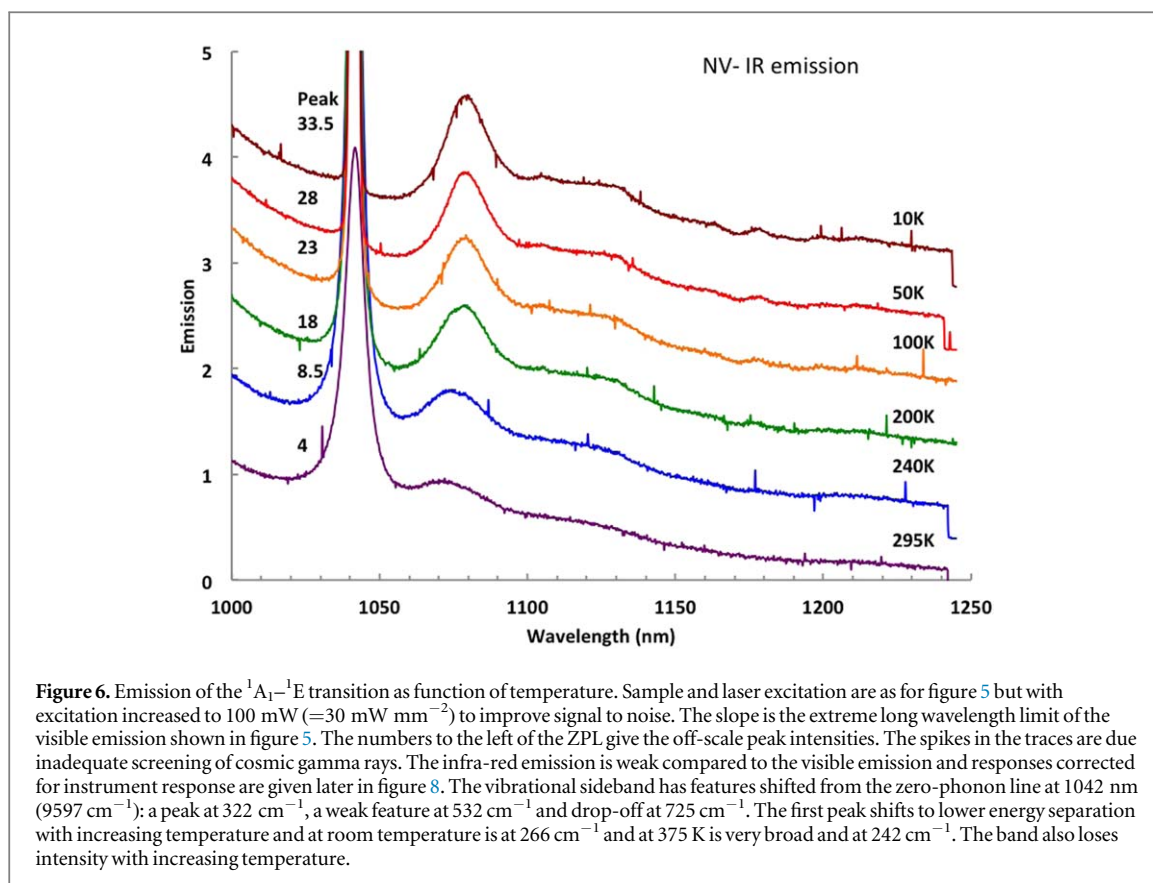

Figure 5. Emission of the $^3A_2$–^3E transition of the NV^- from room temperature to 5 K for the sample as in figure 4. The sample has 0.8 ppm NV^- and 115 ppm N^0. Excitation is 10 mW (=3 mW mm^{-2}) at 532 nm. At lower temperatures the relative strength of the zero-phonon compared to the sideband is incorrect as there is near total absorption at the peak of the zero-phonon line and a fraction of the emission is absorbed.

from the excited ^3E state to singlets and decay within the singlets result in weak $^1A_1$–^1E infra-red emission [22] as shown in figure 6.

3.4. Emission of NV^0 and NV^- samples

1b diamonds generally contain NV in both neutral and negative charge states and consequently samples exhibit emission of NV^0 and NV^-. The magnitude of the emission bands is dependent on excitation wavelength and largely for interest an example is given in figure 7 for a wide range of laser wavelengths. The excitation intensities adopted are modest and do not modify the concentrations of NV^- and NV^0 in the sample. The relative emission intensities of NV^0 and NV^- in the traces are due to variation of the NV^0 and NV^- absorption with excitation

Figure 6. Emission of the $^1A_1$–^1E transition as function of temperature. Sample and laser excitation are as for figure 5 but with excitation increased to 100 mW (=30 mW mm^{-2}) to improve signal to noise. The slope is the extreme long wavelength limit of the visible emission shown in figure 5. The numbers to the left of the ZPL give the off-scale peak intensities. The spikes in the traces are due inadequate screening of cosmic gamma rays. The infra-red emission is weak compared to the visible emission and responses corrected for instrument response are given later in figure 8. The vibrational sideband has features shifted from the zero-phonon line at 1042 nm (9597 cm^{-1}): a peak at 322 cm^{-1}, a weak feature at 532 cm^{-1} and drop-off at 725 cm^{-1}. The first peak shifts to lower energy separation with increasing temperature and at room temperature is at 266 cm^{-1} and at 375 K is very broad and at 242 cm^{-1}. The band also loses intensity with increasing temperature.

Figure 7. Emission of a sample (40 ppm nitrogen, 0.2 ppm NV) at 10 K that contain both NV$^-$ and NV^0 shown for various excitation at wavelengths. The excitation wavelengths are marked by letter L. The emission is only from NV$^-$ when the excitation is in the red >575 nm progressing to predominantly from NV^0 for excitation in the blue. There is near equal excitation at 514 nm and for this excitation the strengths of the zero-phonon lines indicate the relative concentrations of the two NV charge states. The noise on the 637 nm trace is due to instability from hole burning when exciting resonantly within the ZPL. The dashed trace indicates the wavelength dependence of absorption (arbitrary scale) of single-subsitutional nitrogen, N^0.

wavelength. By exciting in the red >600 nm the emission can be restricted to NV$^-$ and in the blue <450 nm largely restricted to NV^0 and this is the approach used to give the individual emission spectra in figures 3 and 5.

3.5. Infrared and non-radiative decay

With excitation in the visible the NV$^-$ centre is excited from the $^3A_2$ ground state to the ^3E excited state. Part of the decay from ^3E gives the visible emission and part of the decay is via the singlets. The decay path via the singlets
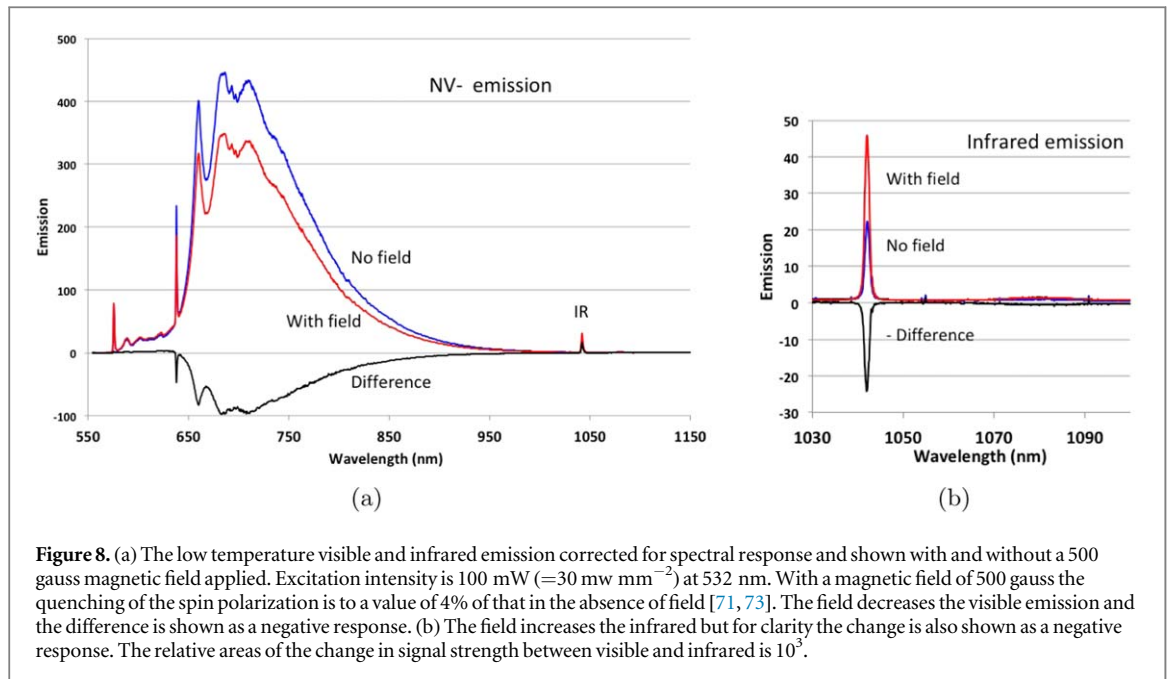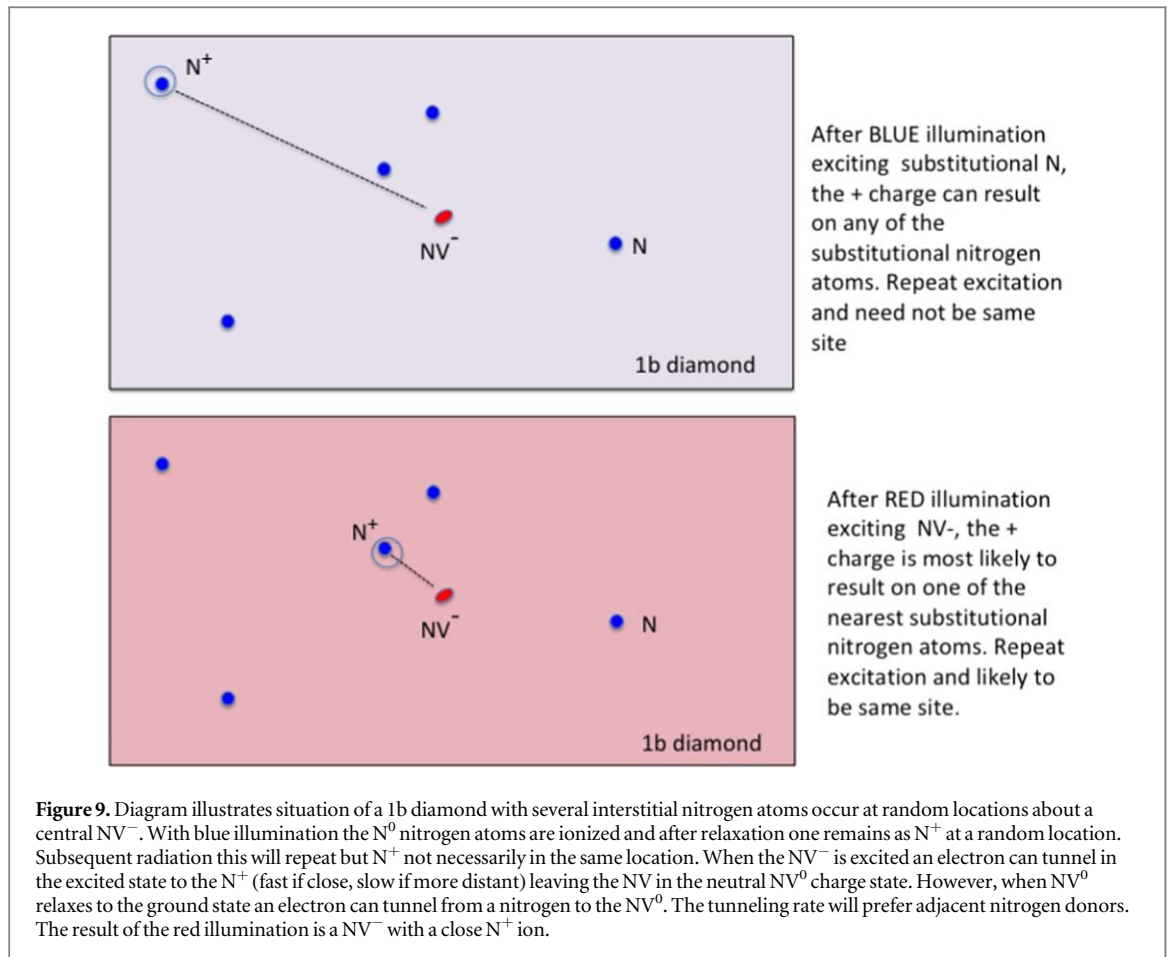
Figure 8. (a) The low temperature visible and infrared emission corrected for spectral response and shown with and without a 500 gauss magnetic field applied. Excitation intensity is 100 mW (=30 mw mm^{-2}) at 532 nm. With a magnetic field of 500 gauss the quenching of the spin polarization is to a value of 4% of that in the absence of field [71, 73]. The field decreases the visible emission and the difference is shown as a negative response. (b) The field increases the infrared but for clarity the change is also shown as a negative response. The relative areas of the change in signal strength between visible and infrared is 10^3.

including the infrared emission gives rise to spin polarization. There is considerable variation in the strength of the infrared emission between samples and this indicates that the spin polarization is not constant. Accounting for the variation in spin polarization is one of the aims of this work.

The inter-system crossing from the ^{3}E to the upper singlet level ^{1}A$_1$ is small for the $m_s = 0$ spin state and large for $m_s = \pm 1$ (values of 0.1 and 1, respectively, are adopted in figure 2). With these inter-system crossing rates optical cycling causes population to be transferred to the $m_s = 0$ spin state and as decay from this state is almost entirely radiative the visible emission is high (and infrared emission low). A magnetic field can be used to quench the spin polarization and reduce this visible emission. For example, a field along $\langle 001 \rangle$ makes an equal angle with the axis of all four orientations of the NV centre and when the field is high the eigenstates have equal contribution of $m_s = 0$ and even when optically excited 33.3% population in the three spin states for each of the four NV$^-$ orientations. The quenching of spin polarization that can be obtained with such a high magnetic field is complete and greater than can be obtained with ground state microwaves as both ground and excited states are effected. The emission is decreased with the application of the magnetic field and the percentage drop is termed as the optical contrast C. Such a measurement for a single centre has obtained contrast of order $C = 40\%$. As there is little inter system crossing from the $m_s = 0$ state when the spin polarization is high and very little of the ^{3}E population decays via the singlets (1% for values used in figure 2). Consequently any emission associated with the ^{1}A$_1$–^{1}E transition in the case of polarized single sites will be weak and infrared emission for single sites has not been detected.

Contrary to the single-site situation, with NV$^-$ ensembles the ^{1}A$_1$–^{1}E infrared emission is readily detectable [22, 23]. The infrared emission can be further increased by applying a magnetic field to quench the spin polarization. Part of the population from ^{3}E is transfered from decaying via the triplets giving the visible emission to decaying via the singlets that includes the infrared emission. The situation is illustrated in figures 8(a), (b) where the signals have been corrected for system response and the changes of the emission introduced by the magnetic field are shown as a negative signal in black. The fraction lost in the visible decay has to be gained by the singlet decay. (There is negligible change to NV^0 emission.) It can be seen that the gain of infrared emission is 10^{-3} of that lost to the visible emission. It is concluded that the infrared decay is largely (by the factor of 10^3) non-radiative. The presence of non-radiative decay was know previously [22] but the determination of the fraction is new. The measurements in figure 8(a) also indicate that for this sample, $\approx$23% of decay from the excited ^{3}E state is via the singlets. This fraction is large compared to the 1% predicted above for single centres.

The increase in the percentage decay via the singlets from the nominal 1% to $\approx$23% is due to vastly different spin polarization. The difference in the degree of spin-polarization between ensembles and single-sites has been recognized previously. For single centres, population in the $m_s = 0$ state has been reported to be in the mid to high 90% [24–27] whereas much lower values are reported for ensembles. Harrison *et al* [28] has measured a value of 78%. Felton *et al* [29] have suggested lower polarization and Drake *et al* [30] has given values as low as

Figure 9. Diagram illustrates situation of a 1b diamond with several interstitial nitrogen atoms occur at random locations about a central NV^-. With blue illumination the N^0 nitrogen atoms are ionized and after relaxation one remains as N^+ at a random location. Subsequent radiation this will repeat but N^+ not necessarily in the same location. When the NV^- is excited an electron can tunnel in the excited state to the N^+ (fast if close, slow if more distant) leaving the NV in the neutral NV^0 charge state. However, when NV^0 relaxes to the ground state an electron can tunnel from a nitrogen to the NV^0. The tunneling rate will prefer adjacent nitrogen donors. The result of the red illumination is a NV^- with a close N^+ ion.

36% for ensembles. The intention in what follows is to identify the process that could account for such significant reduction and for the variation of spin polarization.

4. Tunneling

4.1. $NV^0 -> N^0 \leftrightarrow NV^- -> N^+$ tunneling

The 1b diamonds will have a random distribution of single substitutional nitrogen atoms. After radiation and annealing they will provide the environment for individual NV centres as in the upper schematic in figure 9. The concentration of NV centres can be determined from absorption measurements but what is more significant here is the relative concentration of NV^- and NV^0 centre and this can be determined from the emission spectrum with laser excitation. With low excitation intensities <1 mW mm^{-2} at 532 nm the ratio of NV^0 emission relative to NV^- emission is fixed and for the 115 ppm sample the relative integrated areas of the NV^- and NV^0 ZPL emission gives an NV^0/NV^- ration of the order of 1%. Accepting that the 532 nm excitation is perhaps factor of 2–3 larger for NV^- compared to that for NV^0 the observation implies that a few percent of the NV centres are in the neutral charge state with the fast majority in the negative charge state.

As pointed out by Collins [31], the NV charge state depends on proximity of nitrogen donors. For the 115 ppm N^0 sample the median distance to the nearest nitrogen impurity will be ~3.7 nm. Allowing for a random distribution of N^0 atoms the predominance of negative charge state suggests that for all NV's with an N^0 within about 5 nm an electron will tunnel to give rise to $NV^- - N^+$ pairs. Only the few percent of N^0 out-with this estimate of 5 nm will contribute to the NV^0 population. These are very rough estimates but what is clear is that to obtain the significant fraction in the negative charge state that tunneling of electrons from nitrogen donors N^0 to NV^0 (in the dark) must occur over a few nm's. The specific distances will vary as will the time scales.

With low light levels (<1 mW mm^{-2}) as used in the above measurements, the fraction of NV^0 is not changed and with the 115 ppm case only the few percent of the NV centres are in the NV^0 charge state.
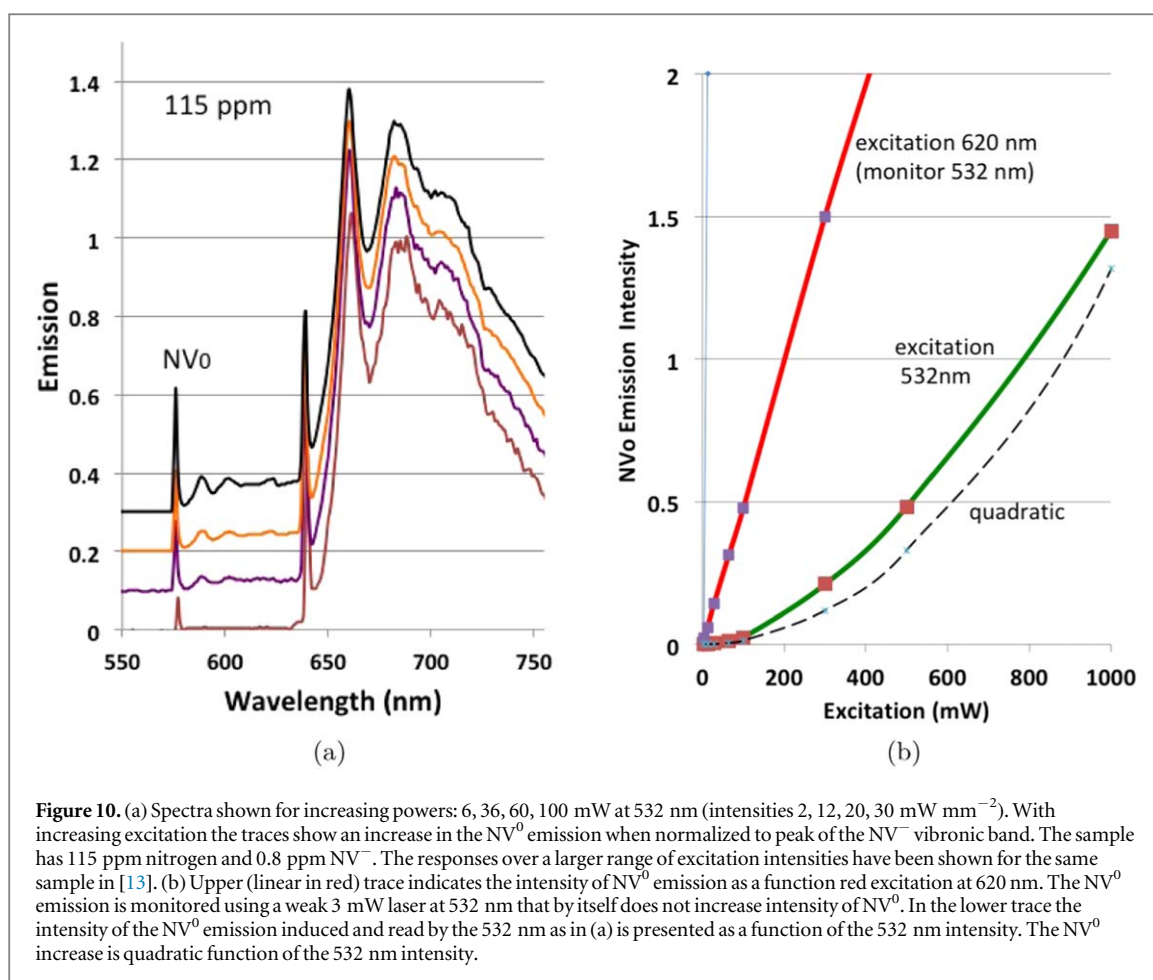
Figure 10. (a) Spectra shown for increasing powers: 6, 36, 60, 100 mW at 532 nm (intensities 2, 12, 20, 30 mW mm^{-2}). With increasing excitation the traces show an increase in the NV^0 emission when normalized to peak of the NV$^-$ vibronic band. The sample has 115 ppm nitrogen and 0.8 ppm NV$^-$. The responses over a larger range of excitation intensities have been shown for the same sample in [13]. (b) Upper (linear in red) trace indicates the intensity of NV^0 emission as a function red excitation at 620 nm. The NV^0 emission is monitored using a weak 3 mW laser at 532 nm that by itself does not increase intensity of NV^0. In the lower trace the intensity of the NV^0 emission induced and read by the 532 nm as in (a) is presented as a function of the 532 nm intensity. The NV^0 increase is quadratic function of the 532 nm intensity.

However, if the optical power is increased the proportion of NV^0 is also increased as shown in figure 10(a). The increase arises from tunneling in the NV$^-$ excited state. The tunneling in the excited state is from NV$^-$–>N$^+$ to give NV^0 and N^0. The increase of NV^0 via this process with red light is linear in excitation intensity as shown in figure 10(b). The latter is measured by exciting with a red laser at 620 nm and monitoring the increase in NV^0 by detecting the emission at 600 nm ($\pm$10 nm) using a weak 3 mW ($=$1 mW mm^{-2}) probe at 532 nm. Should a 532 nm green laser be used to both induce and monitor the NV^0 emission the signal strength is quadratic as shown in figure 10. As intensity is increased $>$300 mW there continues to be some increase in the NV^0 emission but the linear process saturates. Should the photo-ionization with green laser be via the two-photon NV$^-$–>NV^0 process the increase with the increasing read intensity would be cubic. This is not what is observed. The present linear tunneling situation has been reported previously in [13] and illustrated for a larger range of excitation intensities. Ionization of NV$^-$ to NV^0 has also been shown in figure 8 of [15].

The linear tunneling NV$^-$–N$^+$ to attain NV^0 can be observed at intensities orders of magnitude less than that required to detect the two-photon ionization frequently reported in the case of single centres [32]. (At 532 nm two-photon ionization observed at 10^4 W mm^{-2} whereas in general intensities here are $<$10^3 W mm^{-2}). It is recognized that two-photon inter-conversion between NV$^-$ and NV^0 are intrinsic processes associated with the NV centre. When there is no linear processes due to the tunneling rates being too slow with large NV—N separations the two-photon process will be the only mechanism whereby there can be NV$^-\langle-\rangle$NV^0 conversion. With intensities adopted here no significant two-photon processes are observed.

The NV$^-$–>N$^+$ tunneling occurs in the excited state of NV$^-$. As it is only in this state for 13 ns the rates must be fast to have a reasonable probability of tunneling within this time. Also as the rates will decrease exponentially with increasing separation of the NV$^-$–N$^+$ pair, the tunneling with the closest pairs will be favored. At low intensities it will mainly involve the very close pairs but with higher intensities the average time in the excited state can be increased to obtain contributions from more distant pairs. With continuous excitation a NV^0 population can be maintained dynamically and it is this population that is observed for example in figure 10(b). The population attained following a step increase in excitation intensity has been measured previously [13]. When the excitation is switched off the population of NV^0 will not be maintained and all NV^0 will relax to their

ground state. Once in the ground state there will be NV^0–>N^0 tunneling back to give the original NV^- population. The rates for this recovery process has also been measured in previously publication [13]. Both rates, creation and decay, of NV^0 were found to varied from μs to minutes (and the fastest decay rates were probably instrument limited). The scale-free rates are as expected for the enormous range of separations in a bulk crystal and hence the large distribution of tunneling rates. So far it has not been possible to determine rates associate with specific separations.

The tunneling will be a one photon process and in the molecular model as given in figure 2 it is possible that $NV^0(e^2a)$ in the ground state captures an electron from N^0 and tunnels directly to the $NV^-(e^2a^2)$ ground state. However, in the excited state the NV^-–>N^+ tunneling is unlikely to be direct to the $NV^0(e^2a)$ ground state as this would involve a two-electron transition. It is possible, therefore, that the decay from $^3E(e^3a)$ involves tunneling to the meta-stable $^4A_2(e^2a)$ quartet level. However, the specific details of the tunneling transitions requires further theoretical consideration.

The NV^0–>N^0 tunneling in the ground state will favor the faster rates and tunneling from the closest N^0. Hence the optical cycle will create NV^- centres with close N^+ donors. Should this be the only process optical excitation will always generate crystals with a predominance of NV^- centres with close N^+. However, this is not the only process. Optical excitation can also excites N^0 centres throughout the crystal. The excitation can ionize N^0 to give N^+ centres with an electron in the conduction band. The conduction electron will be trapped elsewhere in the lattice and although not the dominant process [33] can occasionally combine with one of the N^+ ions. Should this occur the consequence is that a N^+ is created at a random location and becomes the donor at the expense of the close donor. Therefore, with the optical excitation of substitutional nitrogen atoms there is a redistribution of the location of the N^+ ions with respect to the NV^- centres and the process counteracts the creation of N^+ ions close to the NV^-. This latter process can occur for single sites and give undesirable spectral diffusion [34–37].

It is worthwhile mentioning an alternative process that is possible is where there is ionization of N^0 to create N^+ and the electron released is captured by a NV^0 centre to increase the concentration of NV^- and N^+. There is no evidence of this although the present samples have very low NV^0 concentrations and do not present optimal conditions for detecting such a process. With the samples investigated here this process is not considered further.

5. Visible 637 nm absorption ZPL width

5.1. Absorption line width—no illumination
The competition between the two processes that alter the distribution of N^+ ions results in observable changes of the line width of the low temperature 637 nm ZPL. The processes themselves are not temperature dependent and low temperatures are only necessary as the changes in line width are not observable at higher temperature due to phonon broadening of the ZPL. When the N^+ is close to the NV^- the charge gives a Stark shift of the optical transition that varies from site to site and the combined effect is a broadening of the optical line distinguishable at temperatures <77 K. On the other hand when the single-substitutional nitrogen are ionized and cause the redistribution of more distant N^+ ions the average Stark shift is reduced and the ZPL width becomes narrower. Equilibrium is established between the two processes and for a given sample the balance only depends on the wavelength of excitation. One process varies with the absorption of NV^- and one with absorption of substitutional nitrogen [38, 39] and their variation as function of wavelength are shown in figure 4. Due to the absorption dependence with wavelength the result is a broadening when the 'preparation' excitation is in the red as the wavelength favors NV^- excitation and a narrowing when the 'preparation' excitation is in the blue favoring nitrogen ionization. The situation varies continuously between the red and blue and various intermediate wavelengths are illustrated in figure 11 and also later in figure 18(b). Figure 11 presents a series of transmission measurements of NV^- of the 115 ppm 1b diamond sample at 77 K. Each measurement is the same: a measurement of transmission of the crystal in the spectral range of the $^3A_2$–^3E ZPL from 630 to 650 nm using a low intensity white light source (that does not cause photo-ionization). The transmitted light is dispersed by a monochromator and detected with a photomultiplier. Other than the monitoring light there is no light on the sample at the time of the measurement. Prior to each measurement the sample is exposed to light of a given color. (The wavelengths used are the same as used in figure 7.) The order of the color does not matter and the intensity and duration of exposure are also not of great significance usually being a few milliwatts for 10's of seconds. The wavelength determines the balance. After the light is switched off, relaxation and tunneling is largely complete within a minute. The situation is stable and the absorption can be measured with the low intensity light source. There is no change to the integrated area of the ZPL.
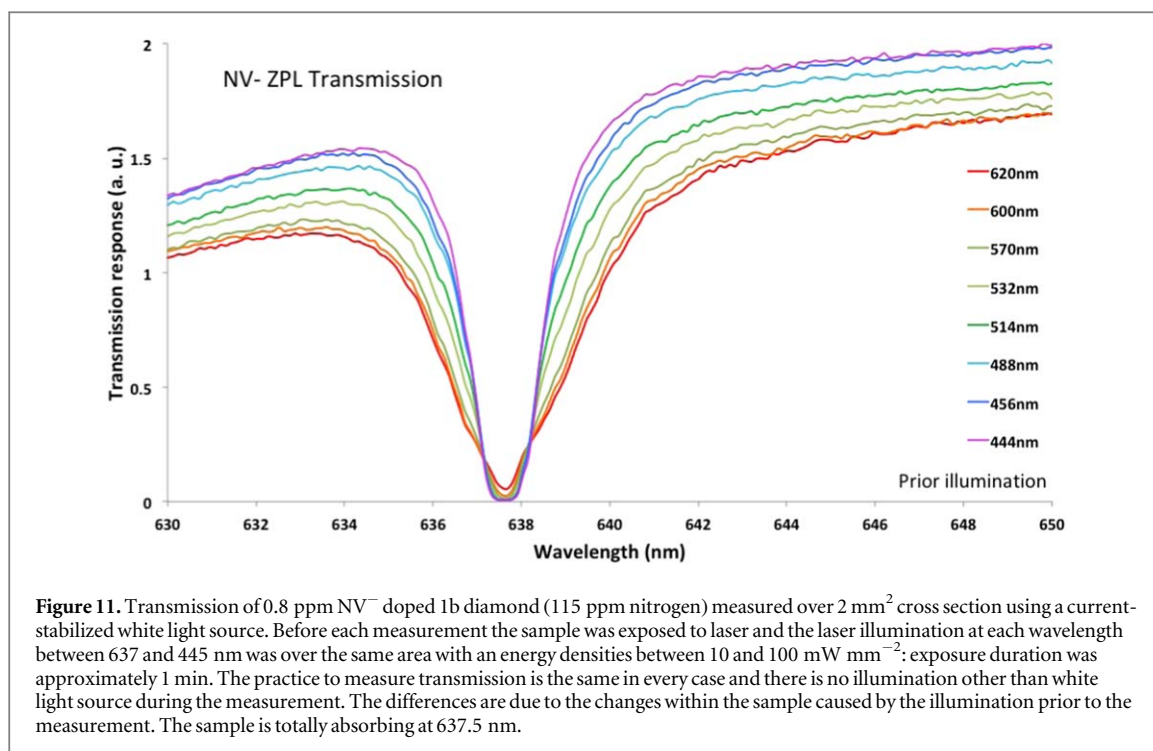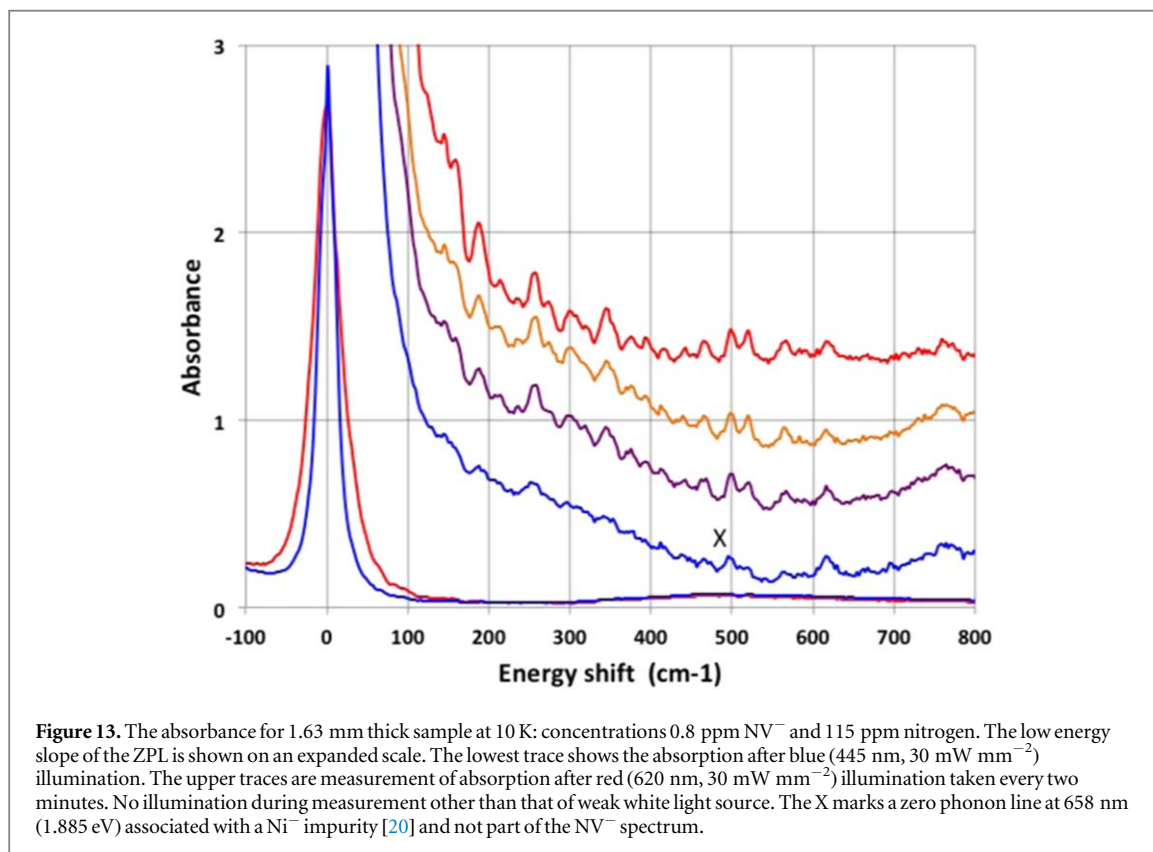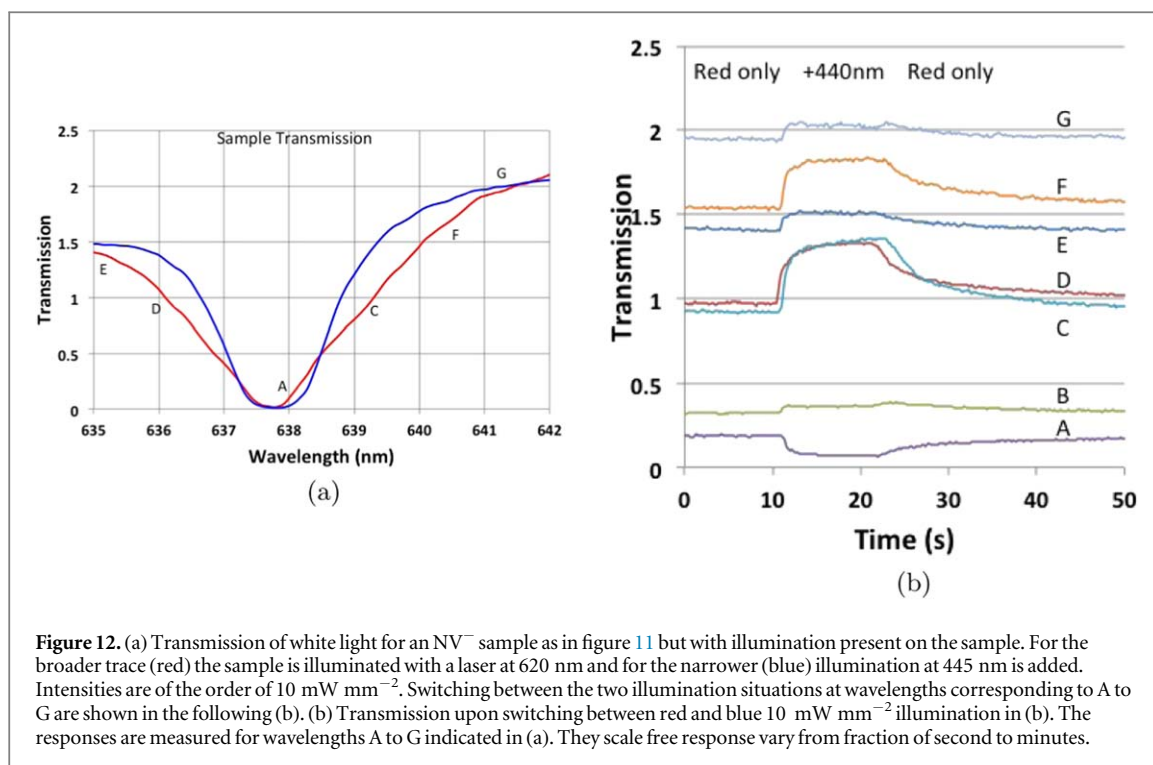
Figure 11. Transmission of 0.8 ppm NV^- doped 1b diamond (115 ppm nitrogen) measured over 2 mm^2 cross section using a current-stabilized white light source. Before each measurement the sample was exposed to laser and the laser illumination at each wavelength between 637 and 445 nm was over the same area with an energy densities between 10 and 100 mW mm^{-2}: exposure duration was approximately 1 min. The practice to measure transmission is the same in every case and there is no illumination other than white light source during the measurement. The differences are due to the changes within the sample caused by the illumination prior to the measurement. The sample is totally absorbing at 637.5 nm.

The above assumes no other possibility for the variation in line width has been considered. Within the optical cycle where the optically induced population of NV^0 decays to the ground state and immediately afterwards there is a recovery of NV^- [13] it is distinctly unlikely that this does not occur with an electron tunneling from N^0 to NV^0. This must favor fast tunneling and the creation of close N^+ ions. The close ion could introduce an extra strain but it is more likely to be the reverse as N^+ has the same electronic structure as carbon and so strain will be minimal. The N^+ replaces a N^0 and so the strain could be reduced but not sufficient to introduce a displacement of the ZPL from the mean. If this was the case there would be a shift of transition frequency that is canceled by the optical cycle not the reverse. There maybe some minor changes in strain but undoubtedly the dominant effect is that of the Stark effect due to the introduction of the positive charges close to the NV^- centres as asserted above.

There is only one previous report of broadening of 637 nm ZPL in single crystal diamond. This is by Nishikori *et al* [40] in relation to a low temperature (60 K) hole burning study. An increase in line width of a 70 ppm nitrogen sample was observed using low temperature hole burning when exciting at or close to resonance at 637 nm. The observations are consistent with that given here. The broadening was considered anomalous and the authors speculated on possible explanations. One of the present authors has included a summary of the broadening effects and given a partial explanation in a book chapter by Zvyagin and Manson in 2012 [41].

5.2. Absorption line width—with illumination

The transmission measurements in figure 11 are made without other light on the crystal during the individual measurements but this is not essential as illumination can be present without changing the observation. The creation of additional N^+ through ionization of the single-substitutional nitrogen does not give absorption. Also there is negligible change to the NV^- ground state population through optical excitation. The result is that simultaneous modest optical illumination (<30 mW mm^{-2}) does not alter the transmitted light intensity. What is interesting is that when both colors are applied simultaneously the narrower line width as occurs for blue only illumination is obtained. This is because tunneling involves slow processes (up to many seconds) and is not competitive with ionization and fast electron migration in diamond. The rates in reaching equilibrium upon switching on red (620 nm) or blue (445 nm) are shown in figures 12(a) and (b). As with previous NV^0 ionization measurements there is a wide range of rates although the techniques adopted for the figures are biased towards observing the slower responses. This variation between red only excitation and simultaneous excitation with red and blue proves invaluable for further investigations and is an approach adopted for many measurements where excitation has to be present such as with emission. Dual excitation allows for the comparison of close N^+ and dispersed N^+ situations.

Figure 12. (a) Transmission of white light for an NV$^-$ sample as in figure 11 but with illumination present on the sample. For the broader trace (red) the sample is illuminated with a laser at 620 nm and for the narrower (blue) illumination at 445 nm is added. Intensities are of the order of 10 mW mm^{-2}. Switching between the two illumination situations at wavelengths corresponding to A to G are shown in the following (b). (b) Transmission upon switching between red and blue 10 mW mm^{-2} illumination in (b). The responses are measured for wavelengths A to G indicated in (a). They scale free response vary from fraction of second to minutes.

Figure 13. The absorbance for 1.63 mm thick sample at 10 K: concentrations 0.8 ppm NV$^-$ and 115 ppm nitrogen. The low energy slope of the ZPL is shown on an expanded scale. The lowest trace shows the absorption after blue (445 nm, 30 mW mm^{-2}) illumination. The upper traces are measurement of absorption after red (620 nm, 30 mW mm^{-2}) illumination taken every two minutes. No illumination during measurement other than that of weak white light source. The X marks a zero phonon line at 658 nm (1.885 eV) associated with a Ni$^-$ impurity [20] and not part of the NV$^-$ spectrum.

5.3. 'Moguls'

As well as Stark broadening of the ZPL as in figure 11 additional features are observed on the low energy side of the ZPL. The features are very irregular on a sloping background termed 'moguls'. These are shown in figure 13. The features are weak but repeatable as shown in the several traces in the figure. After blue (445 nm) illumination the features are small or not present and such a spectrum is shown in the lowest trace of figure 13. The features are more pronounced with red illumination as given by the other three traces. The mogul features are attributed to optical transitions where there are substantial Stark shifts due to the charge of very close N$^+$ ions. In the
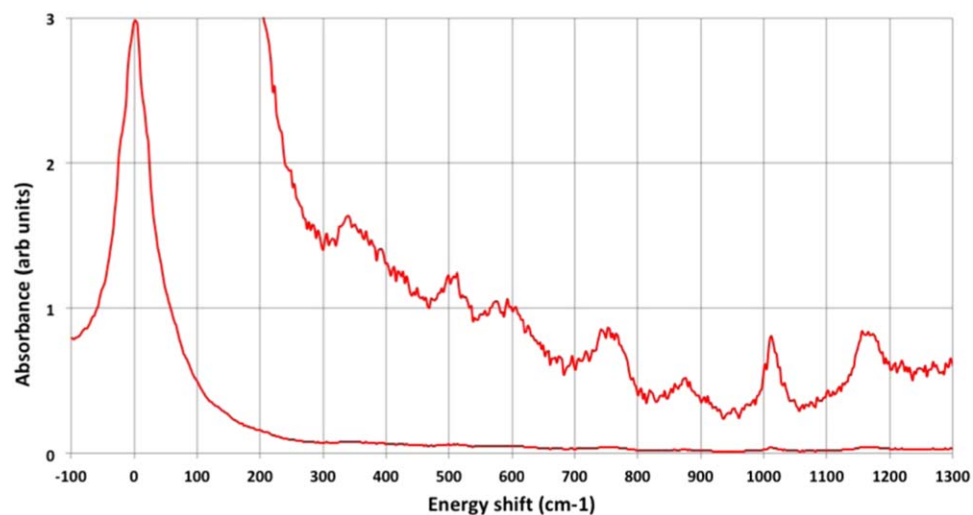
Figure 14. ZPL absorption for a sample with high N^0 and high NV^- concentrations (estimated as 3 ppm and 600 ppm respectively). The upper trace gives the absorbance increased by factor of X 20.

115 ppm nitrogen sample each mogul feature has an optical density of <0.01 compared with the ZPL with an optical density $= 2.5$ (i.e. each mogul has a strength $<1/4\%$ of the parent transition). There is broadening to the high energy side of the ZPL and it is anticipated that there will also be moguls on the high energy side. However, where there is splitting to give energy levels displaced to higher energy the levels will rapidly relax to lower energy and this process will result in broadening. Any such features will not give resolved lines and no distinguishable features are observed. For the lower energy features there are measurement instabilities that leads variation of the background. However, the position of the mogul peaks are reproducible and this aspect is illustrated by repetition of the absorption measurement given in figure 13. (The repetition is given in preference to further averaging as the irregularities still 'looks like' noise.)

The moguls show variation in magnitude due to macroscopic inhomogeneities in the samples. However, the wavelengths of the spectral features are constant and features at the same wavelengths have been observed in both the 115 ppm and the 212 ppm high nitrogen concentration samples. The mogul features were too weak to obtain reliable time dependence although there was indication that the less shifted features develop more slowly than the ones with large shifts. For example in figure 13 a measurement was made at two minute intervals with red illumination after an initial illumination with blue. The magnitude of the lesser shifted feature at 150 cm^{-1} (645 nm) increases slowly with time. In contrast the larger shifted features such as those at 620 cm^{-1} (664 mm) and 780 cm^{-1} (670.7 nm) were more persistent and were still present with the blue illumination. This observation is consistent with the larger shifted features being associated with closer N^+ ions, fast tunneling rates and more resistant to optical induced changes.

A sample with high N^0 and NV^- concentrations was found to give prominent mogul structure that showed little modification with blue light (figure 14). The moguls were significantly broader than those for the 115 and 212 nm samples an aspect attributed to the higher concentrations but the position of the features agreed with those for the other samples. The sample had irregular shape and it was not possible to obtain reliable concentrations from optical absorption and a FTIR measurement. The estimates are 3 ppm NV and 600 ppm N^0. The shifts extended to 690 nm, over 1200 cm^{-1} (150 meV) from the ZPL as shown in figure 14. The observations are attributed to Stark structure associated with a density of charge from NV^- and N^+ giving higher electric fields than can be obtained with a single neighboring charge. There could also be higher electric fields from nickel, Ni^- impurities plus N^+ compensation [17] (see later calculation). The trend associated with the moguls is clear: high density of features close to the parent ZPL at 637 nm adding to the broadening of the ZPL and reduced number of spectral features with increasing Stark shifts.

The observation of moguls requires low temperature. They are distinguishable at 125 K and reach a minimum width by 50 K. This is shown in a series of traces in figures 15(a) and (b).

5.4. Calculation of line broadening and mogul structure

A simple Monte Carlo model was used to calculate the expected broadening and mogul structure due purely from N^+ Stark shifts. For 100 ppm nitrogen and 1 ppm NV^- a volume within 8 nm of a given NV site is considered: a volume involving approximately 10^5 lattice sites. Within this volume each site for 100 ppm N^0 sample has a probability of $1/10^4$ to be a nitrogen atom and each of these nitrogen atoms for 1 ppm NV^- have a
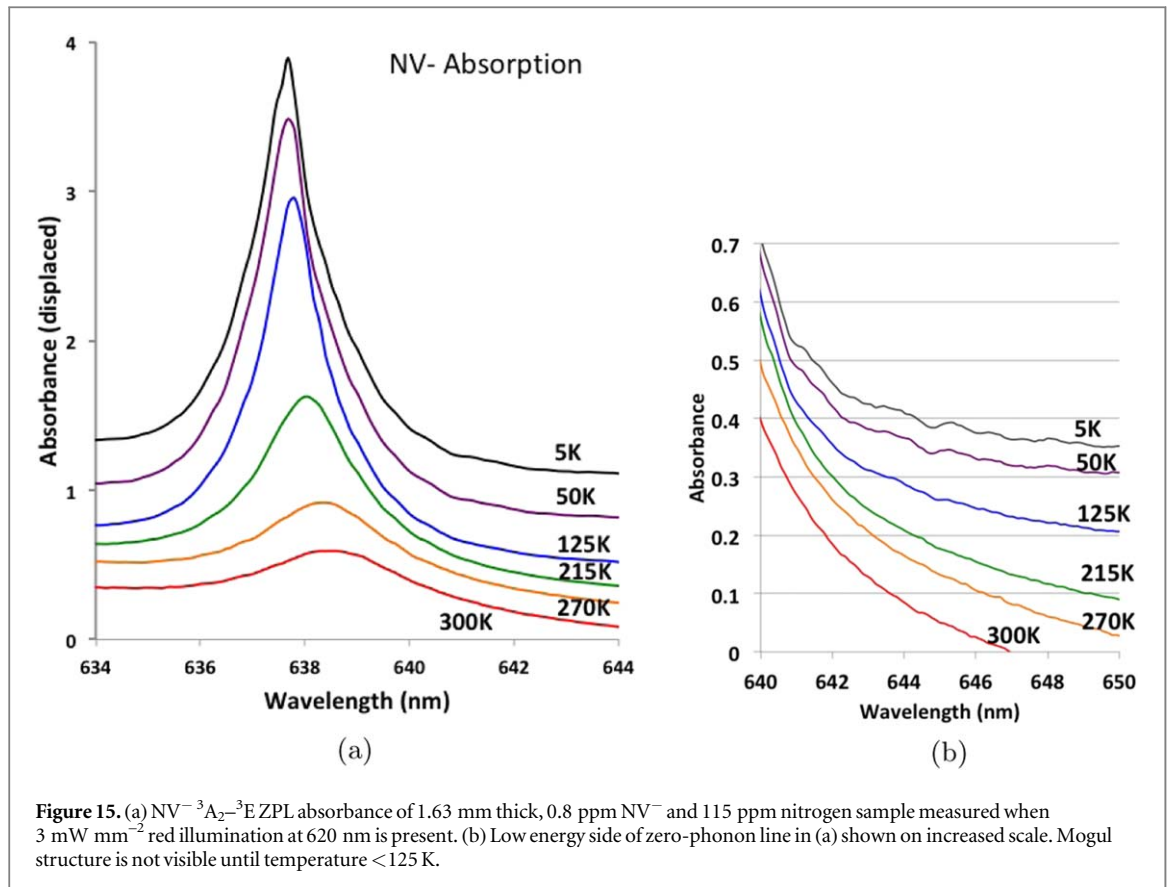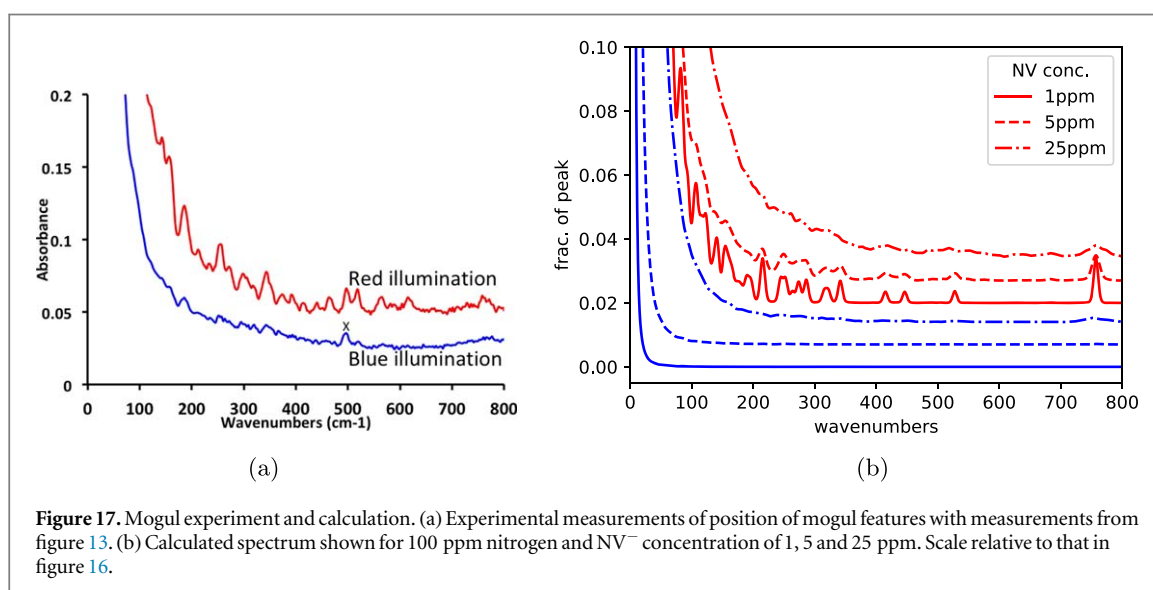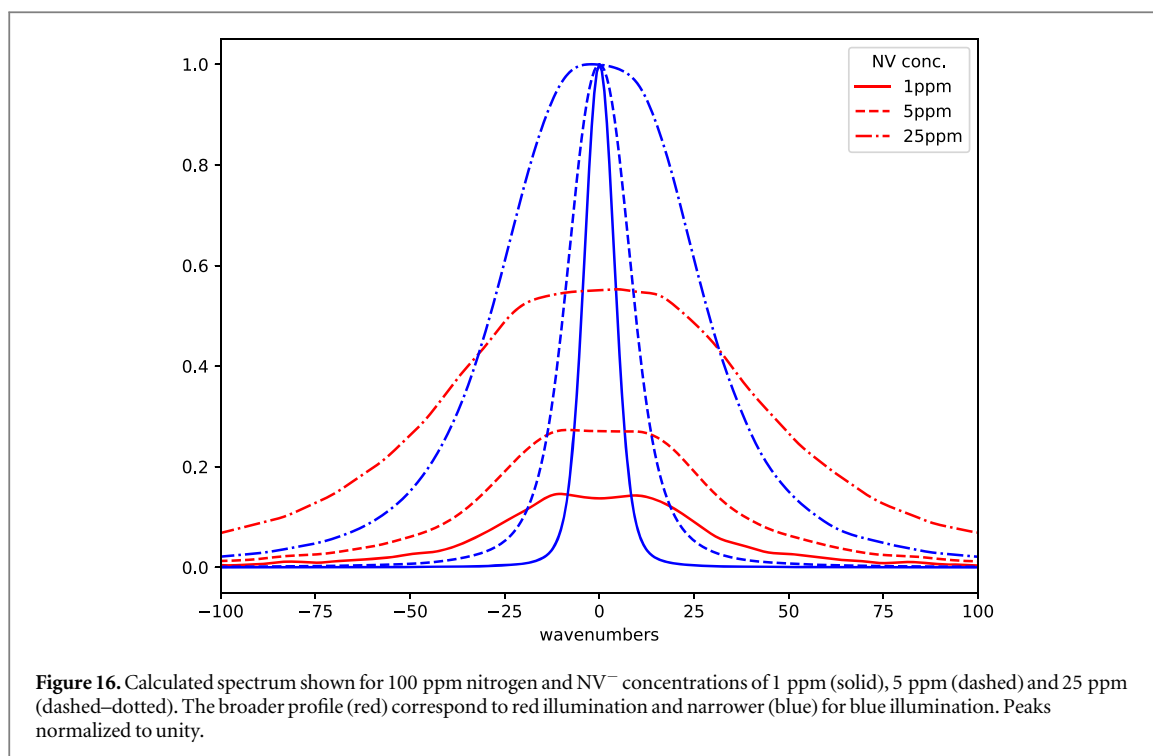
Figure 15. (a) NV$^-$ $^3A_2$–^3E ZPL absorbance of 1.63 mm thick, 0.8 ppm NV$^-$ and 115 ppm nitrogen sample measured when 3 mW mm^{-2} red illumination at 620 nm is present. (b) Low energy side of zero-phonon line in (a) shown on increased scale. Mogul structure is not visible until temperature <125 K.

$1/10^2$ probability to be positively charged. The remaining nitrogen atoms likewise have a $1/10^2$ chance being another NV$^-$ with –ve charge. The electric field at the original NV$^-$ site due to the charges is summed. The site is assumed to contribute two narrow lines to the total, with positions given according to the field sensitivities given by Acosta *et al* [35] (Axial shifts of 4 GHz for 10^4 V cm^{-1} and a splittings of 5 GHz for 10^4 V cm^{-1} although the authors expressed some reservations as only obtained for one centre. Screening due to dielectric constant is included in these values.) Each of the lines is taken to be a Gaussian with width of 0.3 nm, as this is the approximate line width of the narrowest mogul feature. Repeating this calculation 10^5 times and summing the resultant line gives the expected line-shape under blue illumination. For the situation of red illumination, we start with the blue situation already described. If the nitrogen site closest to the NV center is not already charged, then it is made to be charged and one of the charged sites is randomly chosen to be made neutral. The line shapes for these situations are illustrated in figure 16 for 100 ppm nitrogen with NV$^-$ concentrations of 1 ppm. (Results for calculation of 5 and 25 ppm NV$^-$ are also given in the figure.) The central feature is largely determined by the density of charges in the lattice. It is also noted that the central feature is further broadened as the NV$^-$ concentration increases, remembering that there is equal concentration of N$^+$. The mogul structure with shifts >50 cm^{-1} is due to the N$^+$ charges that are close to the central NV$^-$ and the structure is shown in more detail in figure 17(b).

There are a large number of mogul features corresponding to N$^+$ at large distance from the NV$^-$ and these overlap and contribute to the ZPL line width as described above. A shift proportional to the calculated electric field should be valid for such cases as the charge is at large distances (>12 A^0). On the other hand there are a small number of sites that give well shifted mogul spectral features. The approach is less likely to be valid for the close sites as the level of screening becomes questionable. The shift to the shortest wavelength of a mogul in the 115 ppm (or 212 ppm) sample is by 33 nm (at 750 cm^{-1}, 670 nm). The calculation for this case indicates a NV$^-$–N$^+$ separation of order of 3 A^0. In the present calculation closer N$^+$ (<3 A^0) are disregarded. The result of the calculation for other close N$^+$ is summarized in figure 17(b) and this calculation should be compared with the spectra given in figure 17(a) associated with the moguls from the experimental trace in figure 13. There is a reasonable degree of accord and gives support that the principles of the calculation and the mechanisms proposed are correct. Clearly more rigorous calculations are desirable. The weakness is that shifted features cannot yet be associated with specific NV$^-$ N$^+$ separations and there is some uncertainty of the electric field parameters [35]. Without such an information the calculations can only be expected to show the general correspondence rather than agreement.

Figure 16. Calculated spectrum shown for 100 ppm nitrogen and NV$^-$ concentrations of 1 ppm (solid), 5 ppm (dashed) and 25 ppm (dashed–dotted). The broader profile (red) correspond to red illumination and narrower (blue) for blue illumination. Peaks normalized to unity.

Figure 17. Mogul experiment and calculation. (a) Experimental measurements of position of mogul features with measurements from figure 13. (b) Calculated spectrum shown for 100 ppm nitrogen and NV$^-$ concentration of 1, 5 and 25 ppm. Scale relative to that in figure 16.

6. Visible 637 nm emission and excitation ZPL width

6.1. Emission line width

The above analysis of the $^3A_2$–^3E ZPL in absorption has established the dynamics within the crystal that occur with optical illumination and this information is invaluable for the interpretation of emission spectra. Just as the 637 nm absorption line width varies with illumination wavelength, one might expect the emission line width to vary with excitation wavelength. Emission for various wavelengths of excitation is shown in figure 18(a) and for convenience the absorption for the same wavelengths is given in the accompanying figure 18(b). The ZPL in emission is broadest when excitation is in the red and narrowest in the blue and various intermediate wavelengths are also included in figure 18(a). The differences between red and blue responses are conveniently obtained by recording the emission using modulated red excitation with and without simultaneous excitation with blue light (see figures 18(a), 19(a)). The signal in both cases is that of NV$^-$ emission excited by the red (modulated) laser. What is changed is the distribution of N$^+$ caused by the excitation: close N$^+$ in the case of red only excitation and random located N$^+$ when blue is applied simultaneously. These traces are repeated latter in
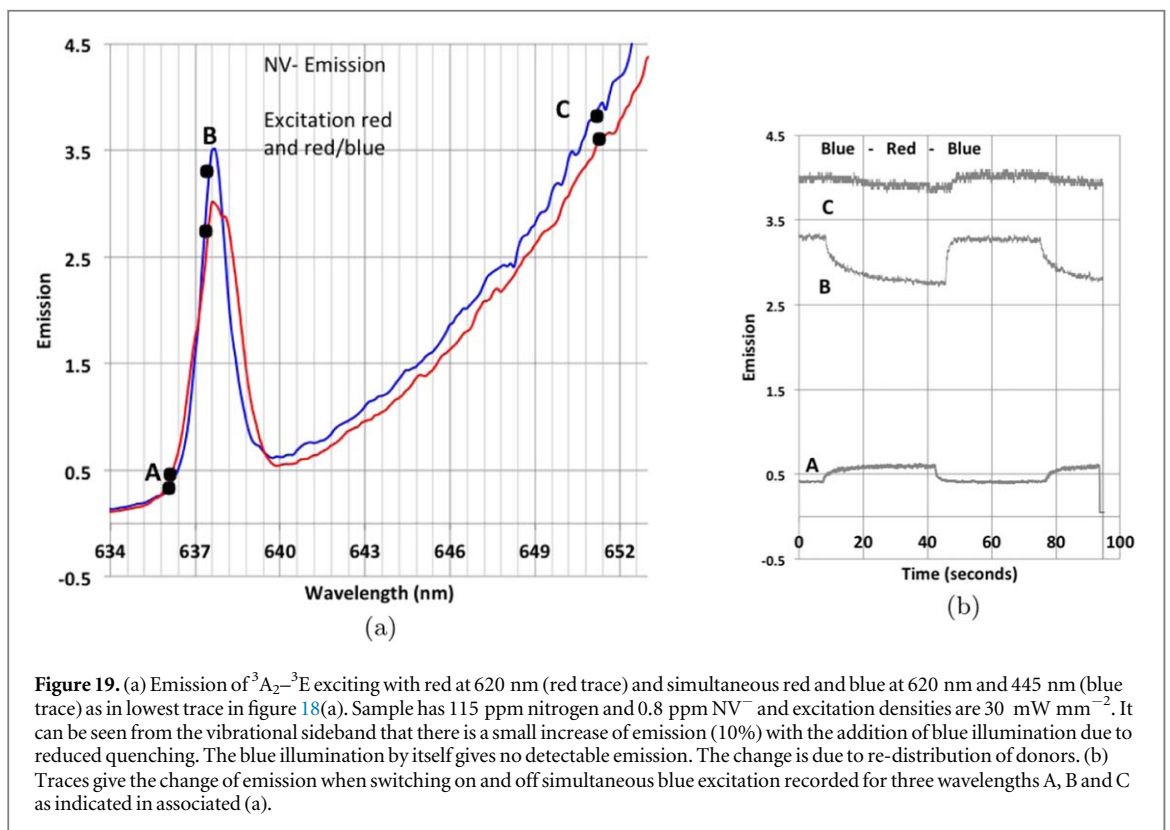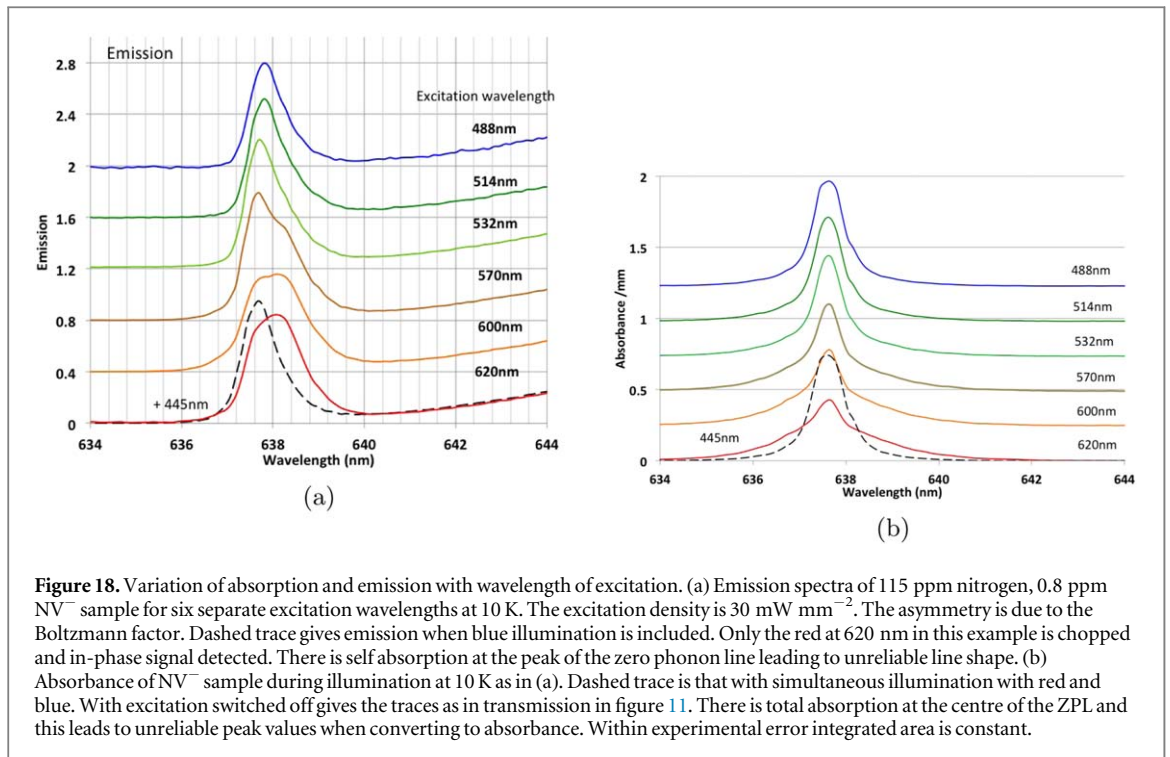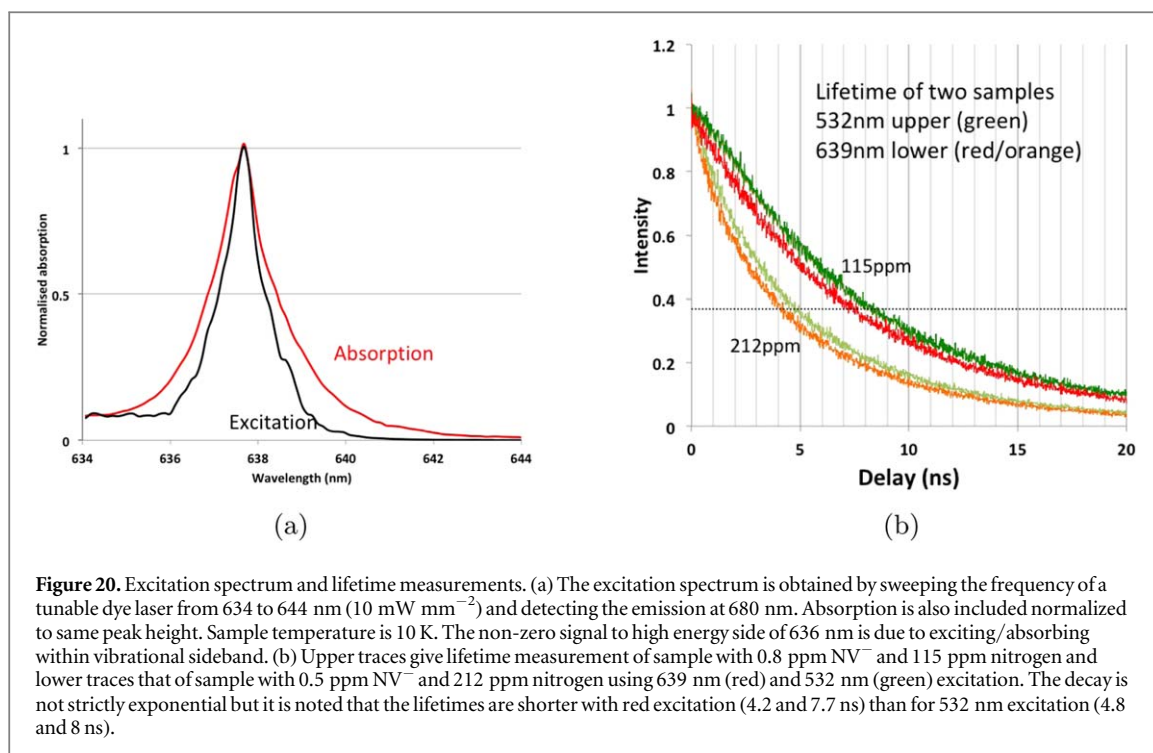
Figure 18. Variation of absorption and emission with wavelength of excitation. (a) Emission spectra of 115 ppm nitrogen, 0.8 ppm NV^- sample for six separate excitation wavelengths at 10 K. The excitation density is 30 mW mm^{-2}. The asymmetry is due to the Boltzmann factor. Dashed trace gives emission when blue illumination is included. Only the red at 620 nm in this example is chopped and in-phase signal detected. There is self absorption at the peak of the zero phonon line leading to unreliable line shape. (b) Absorbance of NV^- sample during illumination at 10 K as in (a). Dashed trace is that with simultaneous illumination with red and blue. With excitation switched off gives the traces as in transmission in figure 11. There is total absorption at the centre of the ZPL and this leads to unreliable peak values when converting to absorbance. Within experimental error integrated area is constant.

Figure 19. (a) Emission of $^3A_2$–^3E exciting with red at 620 nm (red trace) and simultaneous red and blue at 620 nm and 445 nm (blue trace) as in lowest trace in figure 18(a). Sample has 115 ppm nitrogen and 0.8 ppm NV^- and excitation densities are 30 mW mm^{-2}. It can be seen from the vibrational sideband that there is a small increase of emission (10%) with the addition of blue illumination due to reduced quenching. The blue illumination by itself gives no detectable emission. The change is due to re-distribution of donors. (b) Traces give the change of emission when switching on and off simultaneous blue excitation recorded for three wavelengths A, B and C as indicated in associated (a).

figure 19(a) including part of the vibrational sideband. The accompanying figure 19(b) indicate the rate at which the spectra between the two situations change.

6.2. Emission intensity versus wavelength

As well as a difference between red and blue excitation what is more significant is that in all cases the ZPL in emission does not have the extremes of the ZPL measured in absorption. Compare for example spectra given in figures 18(a) and (b) for the case of 620 nm excitation/illumination (lowest traces). Comparison at the central

Figure 20. Excitation spectrum and lifetime measurements. (a) The excitation spectrum is obtained by sweeping the frequency of a tunable dye laser from 634 to 644 nm (10 mW mm^{-2}) and detecting the emission at 680 nm. Absorption is also included normalized to same peak height. Sample temperature is 10 K. The non-zero signal to high energy side of 636 nm is due to exciting/absorbing within vibrational sideband. (b) Upper traces give lifetime measurement of sample with 0.8 ppm NV$^-$ and 115 ppm nitrogen and lower traces that of sample with 0.5 ppm NV$^-$ and 212 ppm nitrogen using 639 nm (red) and 532 nm (green) excitation. The decay is not strictly exponential but it is noted that the lifetimes are shorter with red excitation (4.2 and 7.7 ns) than for 532 nm excitation (4.8 and 8 ns).

frequencies of the ZPL is unreliable owing to self absorption of the emission. Comparison in the wings is more informative and it is seen that there is negligible emission intensity to the high energy side of 636 nm (shift $= +40\,\text{cm}^{-1}$) or low energy side of 639.5 nm (shift $= -50\,\text{cm}^{-1}$) whereas there are responses in absorption (although weak) at these wavelengths. The lack of emission on the high energy side can be due to a Boltzmann factor as measurements are at low temperature (10 K) but this can not explain the lack of emission on the low energy side. Similar information is obtained from the excitation spectrum of the ZPL. There is absorption at wavelengths shorter than 640 nm but at these wavelengths the laser does not give rise to NV$^-$ emission. Hence, the excitation of the ZPL is narrower than the ZPL in absorption (figure 20(a)).

The explanation for the difference between the widths of absorption and emission spectra is due to the fast tunneling in the excited state when the N$^+$ ions are close. NV$^-$ centres can be excited but with fast tunneling to NV^0 the centres do not emit. Therefore, for centres with close N$^+$ and large Stark shifts prevalent with red excitation there will be a loss of radiative decay and a quenching of the emission. There are frequencies that give absorption but little or no emission and it is this fact that results in the more restricted width of the ZPL in emission. The emission lifetime is also shortened and the shortening is again more pronounced with red excitation than with other wavelength such as 532 nm as shown in figure 20(b). The extreme case is that of the mogul features. For NV$^-$ centres contributing to mogul features the N$^+$ are close and there is tunneling in the excited state before any radiative decay. Consequently excitation at the wavelength of the mogul features do not give emission. No emission is detected for wavelengths longer that 640 nm corresponding to an energy shift of $-50\,\text{cm}^{-1}$ implying the centres with NV$^-$–N$^+$ separations of 12 A^0 or closer (see mogul calculation) do not emit. With blue illumination giving the randomly distributed N$^+$ the associated NV$^-$ centres that previously (with red) did not emit are shifted in frequency and now do emit. As a consequence with the addition of blue illumination more centres emit and for the same excitation intensity the total emission is increased by 10%. This is illustrated in figure 19 where the increase is most obvious in the vibrational sideband.

7. Variation with nitrogen concentration

In the above discussion the properties of NV$^-$ in 1b diamond have focused on one nitrogen concentration (115 ppm). It is anticipated that there will be variation of properties with nitrogen concentrations and it will be shown in this section that there are differences that arise as a consequence of changes of the average NV$^-$–N$^+$ separations and the associated tunneling rates.

7.1. Low intensity
Differences between samples with varying nitrogen concentrations can be observed in the emission spectra when using low excitation intensities, <1 mW mm^{-2}. This is illustrated in figure 21 where it can be seen that the

Figure 21. Room temperature emission of NV$^-$ for three concentrations of nitrogen (40, 115 and 212 ppm) using low intensity excitation of 1 mW mm^{-2} at 532 nm. Emission spectra are normalized to peak of vibronic band.
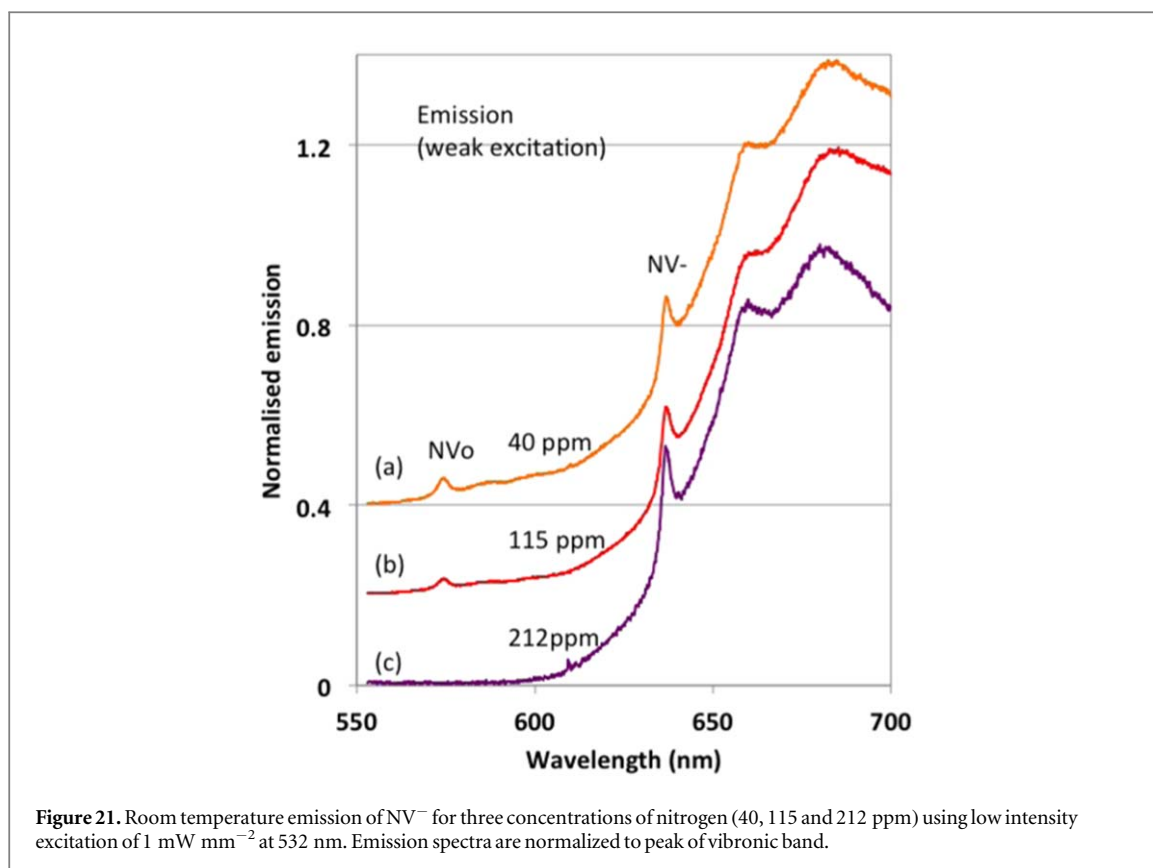
ratio of NV^0/NV$^-$ emission varies with (single substitutional) nitrogen concentration. The variation is a consequence of the different proximity of nitrogen donors altering the tunneling in the ground state. When there is a nitrogen atom within 'reasonable' distance of the NV an electron will tunnel to the NV to give an NV$^-$ centre. When the distances are such that this does not occur within a reasonable time the centre will 'remain' as NV^0 [31]. For the nitrogen concentration of 115 ppm (figure 21) clearly the distance is too large for tunneling for only few percent of the NV centres as discussed in section 4. With lower nitrogen concentration the latter will be more common and for the 40 ppm sample NV^0 there is a factor of three larger number of centres that do not acquire an electron and are neutrally charged. With the higher nitrogen concentration of 212 pm NV^0 does not occur and all centres acquire an electron. The behavior is almost independent of the NV$^-$ concentration, an aspect well illustrated by figure 4 of [42]. Their figure shows spectra for two nitrogen concentrations each with widely varying NV$^-$ concentrations. For low nitrogen concentration (60 ppm) NV^0 is observed for all NV$^-$ concentrations whereas NV^0 is not observed at all with high nitrogen concentrations (200 ppm). The NV$^-$ concentration does have an influence but mainly as it effects the average separation to substitutional nitrogen.

7.2. High intensity

A density of NV^0 (without being optically induced) implies that for some centres in the sample that the tunneling N$^0 ->$NV^0 in the ground state is too slow to create NV$^-$ centres and will be a consequence of large NV—nitrogen separations. This is likely to be an indication of large separations in general in the sample and tunneling in the excited state NV$^- ->$N$^+$ will also be inhibited. If this is the situation and there will only be minimal increase in NV^0 concentration with optical excitation. This the situation for the 40 ppm sample as seen in figure 22(a) (see also figure 8 of [15]). This contrasts with the case of the 115 ppm N^0 sample where there are close N$^+$ ions with fast tunneling and for these centres tunneling in the excited state give rise to the increase in population of NV^0 as reported in the previous section 4 (see figure 10(a)). With higher concentrations such as with the 212 ppm N^0 sample there has to be a much larger fraction of close N$^+$ ions. Larger fraction of ionization and higher NV^0 concentration can be anticipated. However, there is a catch to observing this situation. The tunneling is such that as soon as the NV^0 decays to the ground state it immediately tunnels back to NV$^-$ so that a population of NV^0 cannot be maintained. Therefore in the case of the 212 ppm N^0 sample little NV^0 emission is observed at low intensities and also difficult to detect with higher excitation as illustrated in figure 22(b).

The significant changes in behavior for the 40, 115 and 212 ppm N^0 samples with average NV—N^0 separations varying from 5 to 3.7 to 3 nm is due to the exponential dependence on tunneling rates. As the extent
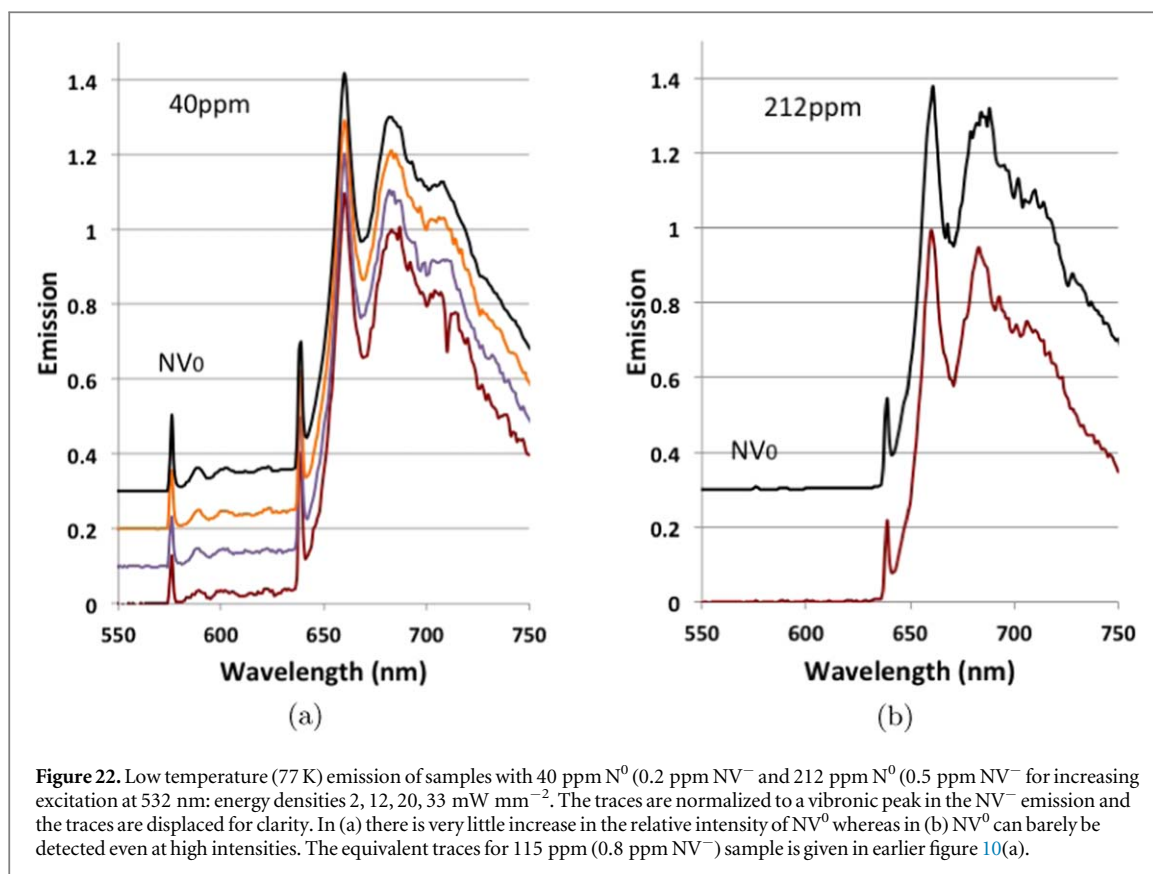
Figure 22. Low temperature (77 K) emission of samples with 40 ppm N^0 (0.2 ppm NV^- and 212 ppm N^0 (0.5 ppm NV^- for increasing excitation at 532 nm: energy densities 2, 12, 20, 33 mW mm^{-2}. The traces are normalized to a vibronic peak in the NV^- emission and the traces are displaced for clarity. In (a) there is very little increase in the relative intensity of NV^0 whereas in (b) NV^0 can barely be detected even at high intensities. The equivalent traces for 115 ppm (0.8 ppm NV^-) sample is given in earlier figure 10(a).

of wave functions drop very rapidly with distance the rates can change by many orders (3–4) of magnitude per nm of $NV-N^0$ separation. The $NV^- -> N^+$ tunneling in excited state requires rates that are comparable to the 10 ns lifetime (maybe 1 ns) and yet $NV^0 -> N^0$ tunneling have to be slow enough in the ground state to allow cycling to enable optical detection of NV^0 emission (maybe μs). There is then a restricted range of tunneling rates that enable the observation of NV^0 with excitation intensity. Although modeling of the situation is desirable the indication is that the fraction of centres matching the condition is optimal for a 100 ppm N^0 sample and less when concentration of nitrogen is either higher or lower.

7.3. Absorption changes

For all three samples with excitation NV^0 centres are creates to different degree. When the excitation is switched off the centres decay and once in the ground state an electron tunnels from the $N^0 -> NV^0$'s to restore the original NV^- population. The tunneling process 'selects' close donors and give Stark broadening of the ZPL. The proportion of centres with close donors and associated broadening is large for the high nitrogen concentrations and small for the low nitrogen concentrations. Regardless of concentration the Stark broadening is reduced when there is a redistribution of donors with blue illumination. Spectra illustrating these trends are illustrated in figure 23.

7.4. Emission changes and lifetimes

In absorption there are differences between the samples with nitrogen concentration. However, the difference in emission with nitrogen concentration is not obvious. This is because the emission of the largest shifted optical frequencies are quenched and so there are frequencies for which there are absorption responses but no emission. The effect is a 'normalizing' of the emission line width and the variation of emission line width with concentration is only just observable. The emission line width of all three samples are similar. (Compare upper traces in figures 23(a), (b) and (c).)

For these three samples the fraction of centres where the emission is quenched and have shorter lifetimes is greater the higher nitrogen concentration. The consequence is that emission lifetimes are faster with the higher nitrogen concentration samples. For example it has been shown earlier in figure 20(b) that the rate for the 212 ppm N^0 sample is faster than for the 115 ppm N^0 sample. Large variation in rates have been reported in the literature and for 1b diamonds the shorter lifetimes correlate with the higher nitrogen concentrations [15, 42–45]. The best illustration is in a recent paper by Bogdanov *et al* [46] where they have shown that for micro-diamonds prepared by HPHT there is a systematic shortening of the lifetime with nitrogen concentration

Figure 23. For all cases the broader traces (red) involve close N^+ ions whereas the broader traces (blue) are for distributed N^+ ions. The upper traces are of emission and the measurements are made with excitation present. In case of the red trace (broad) there is only red excitation at 620 nm. This is chopped and the in-phase emission detected. For the blue trace (narrower) this is repeated but the blue illumination at 445 nm added but not chopped; both intensities 30 mW mm^{-2}. The lower traces give absorbance with peak normalized to unity. Prior to these measurement (red traces) the samples have been illuminated red laser at 620 nm with intensity of 30 mW mm^{-2} for approximately 1 min. This is repeated (blue trace) but with prior illumination with similar intensities at 445 nm likewise for approximately 1 min. All samples at 10 K. (a) 212 ppm (0.5 ppm NV$^-$): emission and absorption. (b) 115 ppm (0.8 ppm NV$^-$): emission and absorption. (c) 40 ppm (0.2 ppm NV$^-$): emission and absorption.

Figure 24. IR ZPL emission of three samples at 10 K. The red trace (no fill) give emission with 30 mW mm^{-2} at 620 nm. The blue trace (with fill) is same excitation at 620 nm but with additional 30 mW mm^{-2} blue illumination at 445 nm. Fill is used to highlight the marginally larger signals in the 'wings' of the line with red excitation. (a) 212 ppm N^0 (0.5 ppm NV$^-$): infrared emission. (b) 115 ppm N^0 (0.8 ppm NV$^-$): infrared emission. (c) 40 ppm N^0 (0.2 ppm NV$^-$): infra red emission.

from 20 ns for 50 ppm nitrogen to 9.5 ns with 600 ppm nitrogen. Associated with shortening of the lifetimes and cycling involving NV^0 there is a reduction of spin polarization and this will be discussed in relation to infrared emission in section 11.

8. Infrared 1042 nm ZPL width

8.1. Infrared line widths

The infrared emission arises from inter-system crossing from the ^{3}E state and when there is visible emission from this state there is also inter-system crossing and infrared emission within the singlets (although weak). It is found that some of the characteristics of the visible emission are also exhibited by the infrared emission. For example, the ZPL at 1042 nm is broader when the excitation is in the red close to the 637 nm ZPL and narrower when there is simultaneous illumination with blue light at 445 nm. Remembering that there is a 'normalizing' of the visible emission with nitrogen concentration and this results in only small variation of the infrared line width with nitrogen concentration. The infrared emission is from an orbital singlet and there is no Boltzmann factor favoring one side of the ZPL as occurs for the visible emission. The result is an infrared ZPL with slight Stark broadening in both 'wings' to high and low energy with little change of the central component. These effects are shown in figure 24 for the three nitrogen concentrations 212, 115 and 40 ppm.
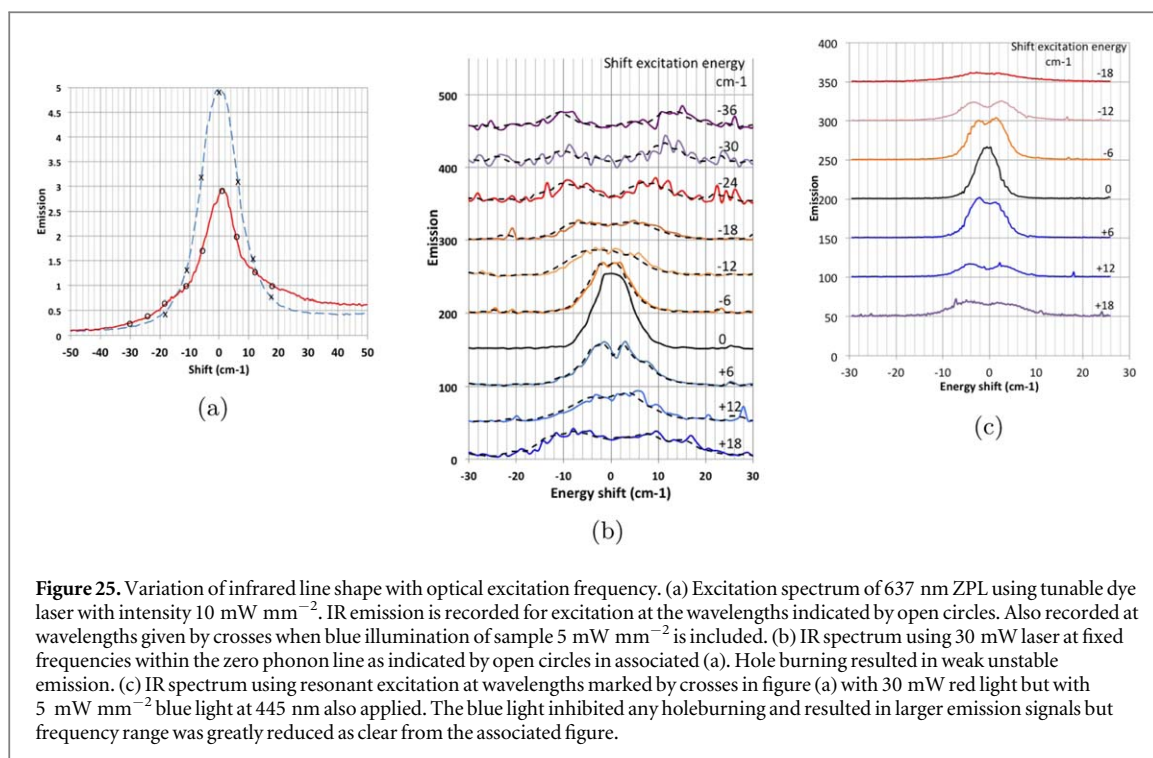
Figure 25. Variation of infrared line shape with optical excitation frequency. (a) Excitation spectrum of 637 nm ZPL using tunable dye laser with intensity 10 mW mm^{-2}. IR emission is recorded for excitation at the wavelengths indicated by open circles. Also recorded at wavelengths given by crosses when blue illumination of sample 5 mW mm^{-2} is included. (b) IR spectrum using 30 mW laser at fixed frequencies within the zero phonon line as indicated by open circles in associated (a). Hole burning resulted in weak unstable emission. (c) IR spectrum using resonant excitation at wavelengths marked by crosses in figure (a) with 30 mW red light but with 5 mW mm^{-2} blue light at 445 nm also applied. The blue light inhibited any holeburning and resulted in larger emission signals but frequency range was greatly reduced as clear from the associated figure.

8.2. Variation of IR ZPL with excitation wavelength

The broadening in figure 24 analogous to the visible (although less) suggests a Stark effect and this was investigated using resonant excitation. A dye laser was tuned to various frequencies (figure 25(a)) within the 637 nm optical ZPL and the IR emission spectrum was recorded for each excitation wavelength. To reduce the loss of emission via hole-burning small random frequency variation of the excitation laser was adopted. The signals although noisy were sufficient to identify structure in the infra red spectrum (figure 25(b)). A splitting of the infrared ZPL was observed and the splitting increased as the excitation is shifted from the central peak at 637 nm. The excitation selects subgroups of centres with specific electric fields and Stark shifts. As a consequence of these electric fields there is a Stark splitting of the infrared transition. The Stark effect for the infrared transition is factor 2.5–3 smaller than that for the optical transition. With illumination of blue light although there is a reduction of the Stark splitting of both visible and infrared, the same ratio of shifts is maintained.

Where the excitation is resonant with the peak of the visible ZPL (0 cm^{-1} in figure 25(a)) there is no splitting of the infrared spectrum (black trace in 25(b)). The infrared acts as a diagnostic and indicates that the visible transition does not exhibit a splitting at this optical frequency. For all other excitation frequencies there is a splitting of the infrared line. A splitting can be expected particularly when the non-axial electric field parameters are larger than the axial parameter. It is concluded from the observations that there is a significant contribution from Stark effects to the infrared line width although no detailed fitting has been attempted.

The 1042 nm line width has been reported previously [47], but the line widths and splittings reported for a sample of <200 ppm nitrogen are more than a factor 2 larger than that given here for the 212 ppm sample (width of 2.4 meV, 19 cm^{-1} compared to <1 meV, 8 cm^{-1} and splittings of 1 meV, 8 cm^{-1} compared to 0.5 meV, 4 cm^{-1}). The explanation could be associate with higher NV$^-$ concentrations or to additional impurities such as with A-centres in the sample discussed in section 12. Should the latter be the situation the widths will be less from a Stark effect and more from random strain as given in their analysis.

9. Optically detected magnetic resonance (ODMR) at 2.87 GHz

9.1. ODMR line shape

Another spectrum that gives a double peak for NV$^-$ in 1b diamond is the ODMR at zero magnetic field. Optical excitation preferentially populates the ground $m_s = 0$ spin state and this is separated from $m_s = \pm1$ by 2.87 MHz. Applying microwaves at this frequency reduces the emission due to the reduction of the spin polarization and the ODMR spectrum is the measure of emission as a function of microwave frequency. For such measurements the samples are within a loop-gap resonator and microwaves are swept through the $m_s = 0$ to $m_s = \pm1$ transitions from 2.86 to 2.88 MHz. The emission is detected at the peak of the vibrational sideband at 680 nm. With excitation of 30 mW mm^{-2} in the red at 620 nm corresponding to the situation of close N$^+$ ions

Figure 26. ODMR of 115 ppm nitrogen sample (0.8 ppm NV⁻) measured at zero field using 30 mW mm^{-2} red excitation at 620 nm (upper traces) and same red excitation but with simultaneous illumination with 5 mW mm^{-2} blue light at 445 nm (lower traces). Vertical response corresponds to reduction of emission. Traces repeated with changed order to ensure no memory effects.
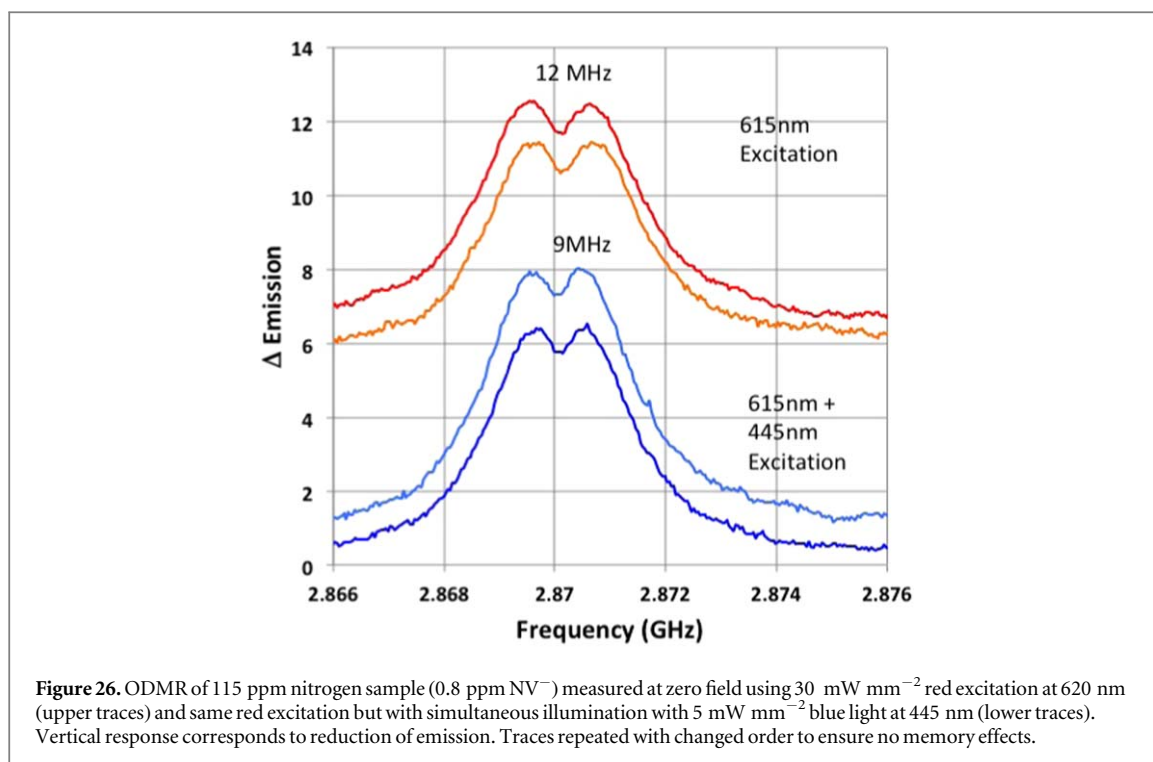
the ODMR response gives a line width of 30 MHz and double peak with separation of 12 MHz as shown in the upper traces in figure 26. When modified to the random N^{+} case by simultaneously irradiating with 5 mW mm^{-2} at 445 nm the ODMR line width is similar but the separation of the double peak is reduce to 9 MHz as given by the lower trace of figure 26. The change in the separation of the double peak suggests that the Stark effect may again play a role in the spectral line shape.

9.2. Variation of ODMR with excitation wavelength

It is found that the ODMR spectrum varies with detection wave length within the ZPL. For example, the separation of the double peak is slightly larger when detection is in the side (high or low) of the ZPL and smaller when the detection is central. Similar observations are obtained using selective excitation at wavelengths within the ZPL and detect emission in the vibrational sideband at 680 nm. A well separated double peak is obtained when the excitation (or detection) is resonant with the wings of ZPL and the double peak is less separated when excitation is central to the ZPL as shown in the traces in figure 27. In both selective excitation and selective emission it is known from the study of the visible ZPL that subgroups of centres experiencing different Stark fields are involved and the observations indicate that the electric fields are indeed playing a role in determining the ODMR spectra. The visible emission widths can be 30 cm^{-1} (900 GHz) (figures 23(b) and 23) and for sensitivities of 4 GHz (axial) and 5 GHz (transverse) for 10^4 V cm^{-1} [35] the widths imply voltages of order of 180.10^4 V cm^{-1}. With spin sensitivity of 0.17 MHz (transverse) for 10^4 V cm^{-1} [48] the present fields can result in ODMR widths of 30 MHz and this is close to the widths observed. This consistency provides additional evidence that Stark effect plays a role in the zero field ODMR line shape. Further investigations with more precise measurement and extended the range of samples are desirable.

The double peak in the ODMR has been reported numerous times and there has been comments that there has been difficulty in fitting to conventional line shapes. The best fit is given by Matsuzaki *et al* [49] and with electric field considered as a parameter. However, fitting line shape where Stark effect is involved is not straightforward as indicated by table 1.

10. Zero-phonon and ODMR line shapes

10.1. Calculations

For all transition, visible ZPL, infrared ZPL and ODMR, it has been shown that Stark effect play a role in giving the line width but in no case has a satisfactory calculation of line shape been completed. The relative positions of the N^{+} ions as attempted in section 5.4 are always required. With knowledge of the Stark parameters the absorption spectra can be calculated and as these are known for the visible transition the line shape can be calculated and the principle for such a calculation has been illustrated in figure 16. All other spectra involve
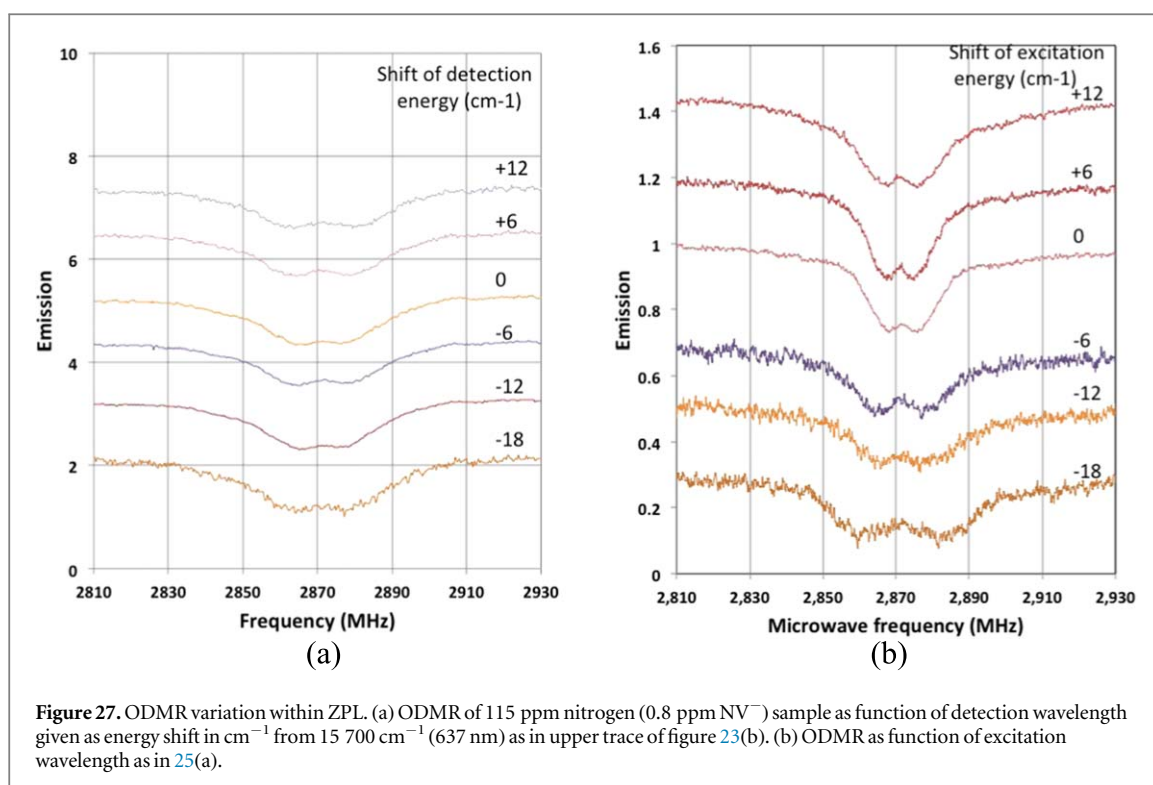
Figure 27. ODMR variation within ZPL. (a) ODMR of 115 ppm nitrogen (0.8 ppm NV^-) sample as function of detection wavelength given as energy shift in cm^{-1} from $15\,700\ cm^{-1}$ (637 nm) as in upper trace of figure 23(b). (b) ODMR as function of excitation wavelength as in 25(a).

Table 1. Parameters required for line shape analysis arising from Stark effect. Z—in all cases it is necessary to calculate the distribution of N^+ about the NV^- centre as made in section 5.4. This enables the magnitude and direction of the electric fields to be determined, Y1—parameters for the Stark shifts of the optical transition at 627 nm are known, Y2—parameters for the Stark shift for the spin transition have been reported, X1—the quenching of emission owing to tunneling in excited state is not known in detail and this effects visible emission intensities, infrared emission intensities and ODMR responses. X2—Stark parameters for IR transitions are not known, X3—The extent to which tunneling affects the reduction of spin polarization is also not known and this can reduce ODMR responses.

Signal	N^0 positions	Vis. Stark	Quenching factor	IR Stark	Spin Stark	Spin contrast
ZPL 637 nm absorption	z	Y1				
ZPL 637 nm emission	z	Y1	X1			
IR 1042 nm emission	z		X1	X		
ODMR at 2.87 GHz	z		X1		Y2	X2

emission and requires knowledge of the quenching effects associated with tunneling rates for the various N^+–NV^- separations. The rates are not known but with such information the visible emission line shapes could be calculated. Likewise the infrared line shape could be calculated although requires different Stark parameters that have yet to be determined. ODMR line requires the information as for the visible emission but in addition a further set of Stark parameters are required. Spin polarization associated with position of N^+ ions also needs to be determined. Calculation of line shapes are clearly complex and the parameters necessary for calculation of the various line shapes are summarized in table 1.

11. Spin polarization and IR emission

11.1. Spin polarization
From the earlier analysis it is recognized that NV^- in the excited state can tunnel to NV^0 and subsequent tunneling in the ground state returns the system to NV^-. This optical cycle involving the charge conversion will not maintain spin polarization and the tunneling will reduce spin polarization attained in a sample. The tunneling is most significant when the NV^- and N^+ ions are close and as such pairs are more common with the higher nitrogen concentrations it is clear there will be a decrease of spin polarization with increasing nitrogen concentration. At very high nitrogen concentrations there are the centres that do not emit, cannot polarize and their presence in samples will further reduce the average spin polarization. This could be the situation with EPR measurements (see [30]). It is concluded that it is the occurrence of excited state tunneling to NV^0 that is the origin of reduced optically-induced spin polarization of NV^- in 1b diamonds.
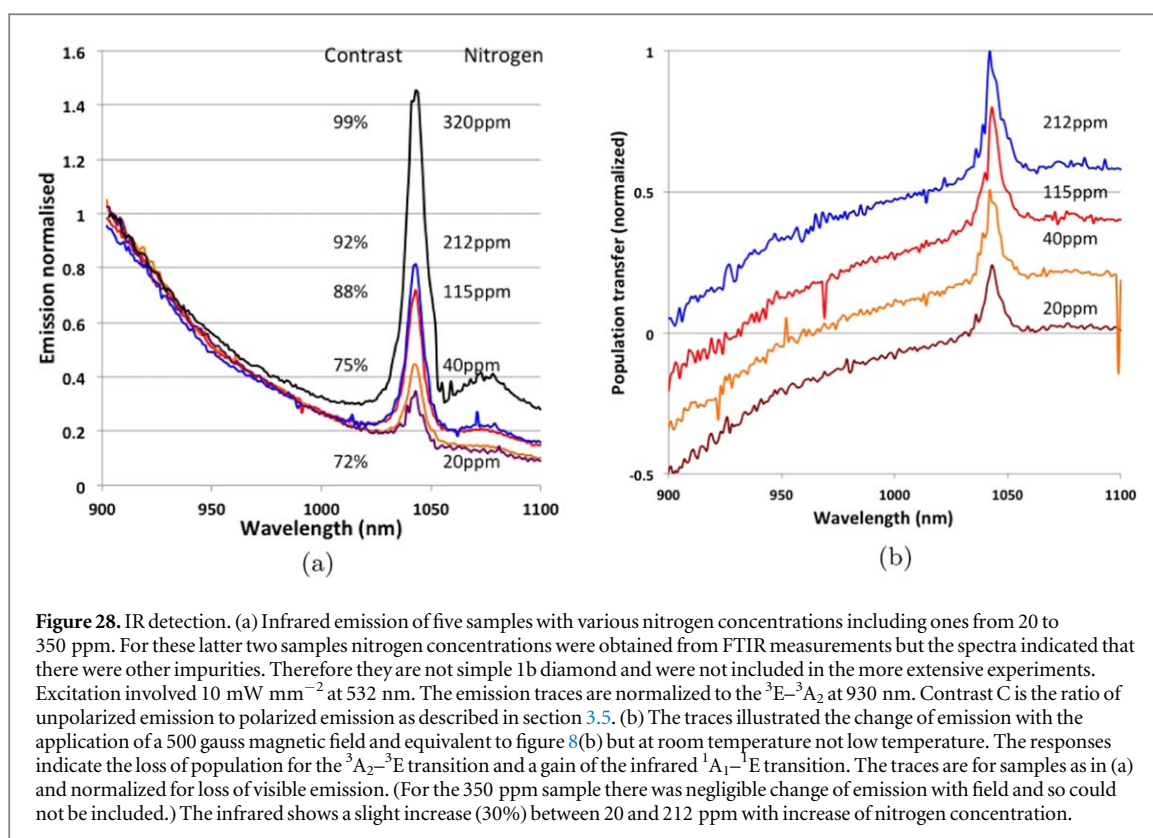
Figure 28. IR detection. (a) Infrared emission of five samples with various nitrogen concentrations including ones from 20 to 350 ppm. For these latter two samples nitrogen concentrations were obtained from FTIR measurements but the spectra indicated that there were other impurities. Therefore they are not simple 1b diamond and were not included in the more extensive experiments. Excitation involved 10 mW mm^{-2} at 532 nm. The emission traces are normalized to the ^3E–$^3A_2$ at 930 nm. Contrast C is the ratio of unpolarized emission to polarized emission as described in section 3.5. (b) The traces illustrated the change of emission with the application of a 500 gauss magnetic field and equivalent to figure 8(b) but at room temperature not low temperature. The responses indicate the loss of population for the $^3A_2$–^3E transition and a gain of the infrared $^1A_1$–^1E transition. The traces are for samples as in (a) and normalized for loss of visible emission. (For the 350 ppm sample there was negligible change of emission with field and so could not be included.) The infrared shows a slight increase (30%) between 20 and 212 ppm with increase of nitrogen concentration.

11.2. Measurement of spin polarization

The reduction of ensemble spin polarization with nitrogen concentration can be conveniently monitored using infrared emission. The fraction of population that decay via the singlet levels and gives rise to the infrared emission increases as the spin polarization is reduced and such a trend is illustrated by figure 28(a). The observation provides a measure of spin polarization of emitting centres. Zero infrared emission corresponds to total polarization with no population in the $m_s = \pm 1$ spin state. On-the-other-hand the signal for no spin polarization can be obtained by applying a magnetic field (approximated by 500 gauss along $\langle 001 \rangle$). Between these limits the singlet emission gives a measure of the polarization. The contrast values in figure 28(a) from 99% to 72% are comparable to those reported in literature and will correspond to a fraction of population in $m_s = 0$ (and $m_s = \pm 1$) varying from and estimated 0.35 (0.65—almost unpolarized) to 0.75 (0.25—high polarized).

The shortcomings of the techniques are recognized. For example to make comparisons requires identical intensities and temperatures. Another experimental issue is that when totally unpolarized as with a magnetic field applied all the samples should give the same ratio between infrared and visible emission as it should only depend on NV$^-$ parameters. However, it is found that there are small differences between samples. The reason is attributed to a small change of the strength of the infrared emission compared to non-radiative decay as illustrated by the traces in figure 28(b). Note the variation in figure 28(a) indicates changes due to the different decay via optical and infra red whereas the variation in figure 28(b) is due to differences in the infrared and non-radiative decay. The latter change is almost certainly due to a variation of the infrared oscillator strength as otherwise it requires the non-radiative transition to become weaker with added nitrogen impurities and this is very improbable. The increasing nitrogen causing a variations of the oscillator strength has intriguing implications for the $^1A_1$–^1E transition and will require further investigation. The effect is 30% and although significant does not make the approach for determining spin polarization from the infrared emission invalid. Further investigations are merited and investigations could also establish whether there is a correlation between optical contrast, optical lifetime and the infrared emission.

12. Discussion

12.1. Samples studied

The range of samples studied is limited. This is as a consequence of the samples not being prepared specifically for this study but rather the study relied on samples available from earlier investigations. The samples of interest are ones containing a concentration of nitrogen but focus on nitrogen that can act as a donor. Only substitutional nitrogen N^0 act as donors, the impurities that formally define 1b diamonds. Hence, the focus is on

NV in 1b diamond with only substitutional nitrogen and there was only the few samples available. Other samples included impurities that were not clearly identified and made any interpretation unsatisfactory. Other impurities may be studied at a later date to establish whether any new physics processes become relevant. There is one exception in that a sample that included A-centres (two nearest neighbor nitrogen atoms) in addition to single substitutional nitrogen was undertaken and reported in the next section 12.5.

12.2. NV$^-$ concentration

A concentrations of NV$^-$ centres can affect properties such as spin polarization but this has not been studied in any detail. No variation of NV$^-$ concentration was available for the samples with substitutional nitrogen. The samples studied had NV$^-$ concentrations of only a few ppm very small compared to nitrogen concentrations of up to several hundred ppm. The present studies can be considered as investigations of *NV interacting with an ensemble of nitrogen atoms* and not to first order *ensembles of NV centres*. Consistent with this the only aspect where the NV$^-$ concentration is shown to influence the properties is that associated with optical line width included within the calculation given in figure 16. The broadening with higher NV$^-$ is only as a consequence of higher electric fields than can be obtained from a single N$^+$ ion. When NV$^-$ concentrations are high there could be Förster resonant energy transfer [50] between NV$^-$ centres and can lead to transfer to a non-emit or non-polarized centre. This process would certainly reduce emission and spin polarization. There could also be energy transfer to the N^0 centres as has been suggested occurs with NV^0 [45], but will be much less for NV$^-$ compared to NV^0 as the absorption strength of N^0 is less at 637 nm compared to that at 575 nm (see figures 4 and 7). In addition at high NV$^-$ densities spin-spin interaction can average the polarization effects as already studied by others [51].

A concentration **n** of NV$^-$ will necessitate crystals with a density of nitrogen and owing to this bath of nitrogen the NV$^-$ centres in the sample will have a range of emission strengths and spin polarizations as indicated in the present studies. Consequently signal strengths will not increase with **n** and signal-to-noise will not increase as $\sqrt{\mathbf{n}}$. It will require samples with a range of NV$^-$ and N^0 to establish which of the process dominate and how signals do vary with NV$^-$ concentration.
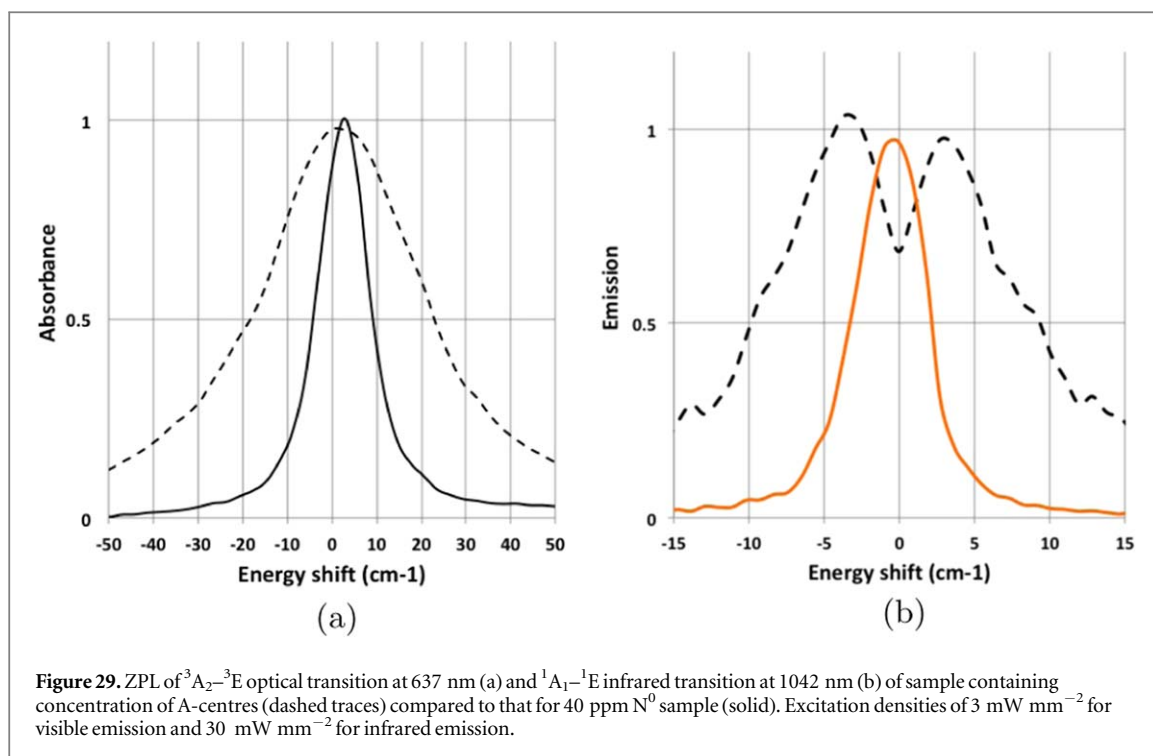
12.3. Spacial

Another aspect not treated concerns the spacial factor. This can be very important when detection is of a very small focused spot such as μ^3 as shown by Jayakumar *et al* [52]. Excitation at one location affects the adjacent environment via diffusion. The situation is avoided in the current study by exciting and detecting mm^3 volume that is relatively large and the effects from the adjacent crystal will be small. Much smaller spot sizes are more relevant for applications and there is a need to investigate how the present observations are modified when the diffusion of electrons and holes into and out of the detected volume as in [52] becomes significant.

12.4. Spin polarization with other impurities

From FTIR measurements (figure 1) it was established that one sample contained nitrogen-pairs (A-centre) in addition to substitutional nitrogen (compare figure 8 in [53]). The A-centres are generally neutrally charged and will not act as donors for NV$^-$ as the ionization energy is 4 eV. The donors associated with the NV$^-$ in this sample will still be the single-substitutal nitrogen atoms (N^0 or C-centres). It is only the N$^+$ ions that can control the spin polarization and when the infrared emission of this sample is compared with other samples it suggests a 'nitrogen' concentration of <100 ppm (not included in figure 28(a)). This is consistent with the measurement of the N^0(C-centre) in the FTIR spectrum in figure 1 but there is a large uncertainty due to the overlap of the A-centre absorption. The assertion is that even in this sample it is the concentration of singly substitutional nitrogen that determines spin polarization but confirmation whether this is always the case requires a wider range of samples.

12.5. Linewidth with A-centre

The presence of the A-centres introduces strain, non-local to the NV$^-$ and this is found to give significant broadening to the electronic transitions in the visible and infrared as shown in figures 29. The broadening from the 192 ppm A-centres is larger than that associated with 212 ppm concentrations of substitutional nitrogen N^0 (C-centres). Indeed the broadening associated with the N^0 (C-centres) is found to be remarkably small as there is little additional width of the optical transition associated with the 212 ppm N^0 sample or the 115 ppm N^0 sample compared to that for the 40 ppm N^0 sample other than that attributed to N$^+$ Stark broadening. Such an observation suggests that the inclusion of the N^0 nitrogen introduces little non-local strain broadening. The best estimate is obtained from the width of the moguls lines where the widths must arise from non-local strain. In the 212 ppm N^0 sample the mogul widths are 4 cm^{-1} (the Stark broadening is 24 cm^{-1}) and this contrasts with 40 cm^{-1} line width for the sample incorporating 192 ppm A-centre nitrogen. It is concluded that the A-centre

Figure 29. ZPL of $^3A_2$–^3E optical transition at 637 nm (a) and $^1A_1$–^1E infrared transition at 1042 nm (b) of sample containing concentration of A-centres (dashed traces) compared to that for 40 ppm N^0 sample (solid). Excitation densities of 3 mW mm^{-2} for visible emission and 30 mW mm^{-2} for infrared emission.

introduces more strain than the N^0. This is not what was anticipated as the single nitrogen substitutes for carbon but undergoes a distortion and the distortion is thought to introduce strain. The normal consideration of strain as treated by Stoneham [54] is from such defects and the strain field is over a volume within the crystal and affect many centres. Davies [55, 56] has treated optical line widths in diamond largely involved natural diamonds where A-centres would be the predominant nitrogen impurity. It is from his analysis that it has been concluded that nitrogen impurities contributed the dominant broadening of ZPL's in diamond samples. This maybe the case but it should be clarified as to which nitrogen impurities introduce the more significant broadening. Ideally an expanded study of line widths for all types of impurities would be worthwhile.

12.6. Other color centres

Photo-conversion between charge states of defects in diamond has been reported many times and long before this or our earlier work [20]. The processes are generally linear and must occur through some type of tunneling or charge hoping. It would be interesting to investigate whether the specific tunneling phenomenon reported here associated with N^+ ions occur in other centres in diamond. For example, there are silicon-vacancy centres SiV^- (ZPL at 738 nm, 1.68 eV) [57, 58] and SiV^0 (ZPL at 946 nm, 1.31 eV) [59], A-centre-vacancy centres H2 (NNV^- at 989 nm, 1.25 eV) and H3 (NNV^0 at 503 nm, 2.46 eV) [56] and vacancy centres GR1 (V^0 at 741 nm, 1.56 eV) and ND1(V^0 at 340 nm, 2.37 eV) [20]. These centres exhibit photo-conversion between the charge states and the extra electron charge may well arises from single substitutional nitrogen. Questions arise as to whether charged ions can become adjacent in these other centres and give Stark broadening as observed here.

12.7. Spin studies

There are many investigations of the spin properties of the NV^- centres including ones associated with ensembles that have relevance to the present optical study. For example Choi *et al* [51] in investigating the spin lifetime and decoherence of NV^- have attributed the degrading of the spin properties to interaction with a fraction of NV^- centres that are not spin polarized, termed 'fluctuators'. The non-polarized NV^- centres may be related to the optical cycle explained here where NV^- are formed from NV^0 by tunneling as such NV^- centres will not be spin polarized. In a separate study of nano-diamonds the spin polarization as indicated by the magnitude of spin contrast has been correlated with optical emission lifetimes [60]. This is a relationship where preliminary measurements have been undertaken here in relation to infrared emission in section 11. Loretz *et al* [61] in studying spin transfer for NV^- to P1 (N^0) at 51 mT in a sample with 77 ppm nitrogen have observed a low spin polarization and saturation of the EPR signal at modest intensities. The authors attribute to the loss of signal and polarization to tunneling from the photo-excited NV^- to adjacent donors consistent with processes proposed in this paper.

12.8. Optical studies of nano-diamonds

In a study of NV^- in nano-diamonds created from 1b diamonds Wolters *et al* [62] observed fast frequency changes of the 637 nm ZPL upon optical excitation and attributed the spectral diffusion to Stark shifts. The processes are associated with the excitation and they rule out two-photon processes. It was notable that the rates observed change with excitation wavelength—faster at higher energies. Their observations are consistent with present measurements. Related to these effects Jamonneau *et al* [63] reported electric field fluctuation that contributed to the noise in the measurement of spin coherence of NV^- in single spin systems. In a very different experiment Bradac *et al* [64] and Inam *et al* [65] have investigated very small nano-diamonds. They observed the emission of small nano-diamonds can be weak and exhibit blinking. The blinking in their cases are most likely related to surface effects as surfaces are a major concern in small diamonds. However, in very small diamonds there is the question whether it is possible to ever have a small number of close NV^-–N^+ pairs that do not emit and give blinking. One can also speculate that there could be issues with close donors when trying to fabricate NV^- centres very close to the diamond surface as achieved by Ofor-Okai *el al* [66].

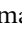## 13. Conclusions

The conclusions are as follows:

1. The spin polarization that can be attained with NV^- centres in 1b diamond is limited by the concentration of substitutional nitrogen.

   - The process that limits the spin polarization is tunneling in the NV^- excited state to NV^0: linear in optical excitation.

2. The properties of the separate centres in 1b diamond depend on NV^-–N^+ separations.

   - When the separation is large the NV^-–N^+ pair centre has properties as reported for NV^- single sites.
   - When the separation is reduced the emission is weaker and spin polarization is reduced.
   - When separation is less than 12 A^0 the pair centre does not emit and clearly there is no spin polarization.

3. Optical excitation alters the NV^-–N^+ separations and with this the properties of the sample.

   - Every observation depends on the excitation wavelength.

4. The N^+ donor gives an electric field at the NV^- site that causes a Stark shift of the spectral transitions within the NV^- system; optical, infrared and spin.

   - The Stark effect in itself is of no particular significance for applications and the details are largely of academic interest. However, it is the study of the Stark effects that provides the vital insight into the properties and changing properties of the NV^-–N^+ pair centre within 1b diamond.
   - The vast majority of the study focuses on the variation of Stark effect on the electronic and spin transitions. Study involves nitrogen concentrations from 320 to 20 ppm. Processes will occur at lower concentrations but could be harder to prove.

5. No significant attention has been given to nano-diamonds, shallow implants or single sites but the knowledge of processes not previously considered may have implications in this wider area. It has to be realized that what are termed as 'NV$^-$ single sites' are in fact NV^-–N^+ pairs where extremely low concentration nitrogen samples have to be adopted to ensure the N^+ are at large distances to avoid the deteriorating factors illustrated in this work.

6. Most significantly the insight into the properties and processes associated with NV^- in 1b diamond will enable better optimization of samples for applications.

ORCID iDs

Neil B Manson © https://orcid.org/0000-0002-5875-4118
Morgan Hedges © https://orcid.org/0000-0001-9714-7356
Michael S J Barson © https://orcid.org/0000-0003-0247-5619
Rose Ahlefeldt © https://orcid.org/0000-0002-2006-2941
Marcus W Doherty © https://orcid.org/0000-0002-5473-6481
Hiroshi Abe © https://orcid.org/0000-0001-9659-8382
Takeshi Ohshima © https://orcid.org/0000-0002-7850-3164

References

[1] Doherty M W, Manson N B, Delaney P, Jelezko F, Wrachtrup J and Hollenberg L C L 2013 The nitrogen-vacancy centre in diamond *Phys. Rep.* **528** 1–45

[2] Rondin L, Tetienne J-P, Tingant T, Roch J-F, Maletinsky P and Jacques V 2014 Magnetometry with nitrogen-vacancy defects in diamond *Rep. Prog. Phys.* **77** 056503

[3] Schirhagl R, Chang K, Loretz M and Degen C L 2014 Nitrogen-vacancy centers in diamond: nanoscale sensors for physics and biology *Annu. Rev. Phys. Chem.* **65** 83

[4] Degen C L 2008 Scanning magnetic field microscope with a diamond single-spin sensor *Appl. Phys. Lett.* **92** 243111

[5] Stanwix P L, Pham L M, Maze J R, Le Sage D, Yeung T K, Cappellaro P, Hemmer P R, Yacoby A, Lukin M D and Walsworth R L 2010 Coherence of nitrogen-vacancy electronic spin ensembles in diamond *Phys. Rev. B* **82** 201201

[6] Shao L, Liu R, Zhang M, Shneidman A V, Audier X, Markham M, Dhillon H, Twitchen D J, Xiao Y-F and Loncar M 2016 Wide-field optical microscopy of microwave fields using nitrogen-vacancy centers in diamonds *Adv. Opt. Mater.* **4** 1075

[7] Glenn D R, Bucher D B, Lee J, Lukin M D, Park H and Walsworth R L 2018 High resolution magnetic resonance spectroscopy using solid-state spins *Nature* **555** 351–4

[8] Tetienne J P, Dontschuk N, Broadway D A, Stacey A, Simpson D A and Hollenberg L C L 2017 Quantum imaging of current flow in graphene *Sci. Adv.* **3** e1602429

[9] Le Sage D, Arai K, Glenn D R, DeVience S J, Pham L M, Rahn-Lee L, Lukin M D, Yacoby A, Komeili A and Walsworth R L 2013 Optical magnetic imaging of living cells *Nature* **496** 486

[10] Glenn D R, Lee K, Park H, Weissleder R, Yacoby A, Lukin M D, Lee H, Walsworth R L and Connolly C B 2015 Single-cell magnetic imaging using a quantum diamond microscope *Nat. Methods* **12** 736

[11] Glenn D R, Fu R R, Kehayias P, Le Sage D, Lima E A, Weiss B P and Walsworth R L 2017 Micrometer-scale magnetic imaging of geological samples using a quantum diamond microscope *Geochem. Geophys. Geosyst.* **18** 3254

[12] Fu R R *et al* 2017 Evaluating the paleomagnetic potential of single zircon crystals using the Bishop Tuff *Earth Planet Sci. Lett.* **458** 1

[13] Manson N B and Harrison J P 2005 Photo-ionisation of the nitrogen-vacancy center in diamond *Diam. Relat. Mater.* **14** 1705–10

[14] Lawson S C, Fisher D, Hunt D C and Newton M E 1998 On the existence of positively charged single-substitutional nitrogen in diamond *J. Phys.: Condens. Matter* **10** 6171

[15] Acosta V M *et al* 2009 Diamonds with high density of nitrogen-vacancy centers for magnetometry applications *Phys. Rev. B* **80** 115202

[16] Hauf M V *et al* 2014 Addressing single nitrogen-vacancy centers in diamond with transparent in-plane gate structures *Nano Lett.* **14** 2359

[17] Davies G 1999 Current problems in diamond: towards a quantitative understanding *Physica* B **273** 15

[18] Davies G 1979 Dynamic Jahn–Teller distortions at trigonal optical centres in diamond *J. Phys. C: Solid State Phys.* **12** 2551–66

[19] Felton S, Edmonds A M, Newton M E, Martineau P M, Fisher D and Twitchen D J 2008 Electron paramagnetic resonance studies of the neutral nitrogen vacancy in diamond *Phys. Rev. B* **77** 081201

[20] Zaitsev A M 2001 *Optical Properties of Diamond* (Berlin: Springer)

[21] Davies G and Hamer M F 1976 Optical studies of the 1.945 eV vibronic band in diamond *Proc. R. Soc.* A **348** 285

[22] Rogers L J, Armstrong S, Sellars M J and Manson N B 2008 Infrared emission of the NV centre in diamond: Zeeman and uniaxial stress studies *New J. Phys.* **10** 103024

[23] Acosta V M, Jarmola A, Bauch E and Budker D 2010 Optical properties of the nitrogen-vacancy singlet levels in diamond *Phys. Rev. B* **82** 201202

[24] Childress L, Dutt M V G, Taylor J M, Zibrov A S, Jelezko F, Wrachtrup J, Hemmer P R and Lukin M D 2006 Coherent dynamics of coupled electron and nuclear spin qubits in diamond *Science* **314** 281

[25] Neumann P *et al* 2010 Quantum register based on coupled electron spins in a room-temperature solid *Nat. Phys.* **6** 249

[26] Togan E *et al* 2010 Quantum entanglement between an optical photon and a solid-state spin qubit *Nature* **466** 730

[27] Robledo L, Childress L, Bernien H, Hensen B, Alkemade P F A and Hanson R 2011 High-fidelity projective read-out of a solid-state spin quantum register *Nature* **477** 574

[28] Harrison J, Sellars M J and Manson N B 2006 Measurement of the optically induced spin polarization of N–V centres in diamond *Diam. Relat. Mater.* **15** 586–8

[29] Felton S, Edmonds A M, Newton M E, Martineau P M, Fisher D, Twitchen D J and Baker J M 2009 Hyperfine interaction in the ground state of the negatively charged nitrogen vacancy center in diamond *Phys. Rev. B* **79** 075203

[30] Drake M, Scott E and Reimer J A 2016 Influence of magnetic field alignment and defect concentration on nitrogen-vacancy polarization in diamond *New J. Phys.* **18** 013011

[31] Collins A T 2002 The Fermi level in diamond *J. Phys.: Condens. Matter* **14** 3743–50

[32] Aslam N, Waldherr G, Neumann P, Jelezko F and Wrachtrup J 2013 Photo induced ionization dynamics of the nitrogen vacancy defect in diamond investigated by single shot charge state detection *New J. Phys.* **15** 013064

[33] Ulbricht R, van der Post S T, Gross J P, Briddon P R, Jones R, Khan R U A and Bonn M 2011 Single substitutional nitrogen defects revealed as electron acceptor states in diamond using ultrafast spectroscopy *Phys. Rev. B* **84** 165202

[34] Bassett L C, Hermanns F J, Yale C G, Buckley B B and Awschalom D D 2011 Electric tuning of single nitrogen vacancy center optical transitions enhanced by photoinduced fields *Phys. Rev. Lett.* **107** 266403

[35] Acosta V M *et al* 2012 Dynamic stabilization of the optical resonances of single nitrogen-vacancy centers in diamond *Phys. Rev. Lett.* **108** 206401

[36] Siyushev P, Pinto H, Voros M, Gali A, Jelezko F and Wrachtrup J 2013 Optically controlled switching of the charge state of single nitrogen-vacancy centers in diamond at cryogenic temperatures *Phys. Rev. Lett.* **110** 167402

[37] Chu Y *et al* 2014 Coherent optical transitions in implanted nitrogen vacancy centers *Nano Lett.* **14** 1982

[38] van Enckevort W J P and Versteegen E H 1992 Temperature dependence of optical absorption by the single-substitutional nitrogen donor in diamond *J. Phys.: Condens. Matter* **4** 2361

[39] Iakoubovskii K and Adriaenssens G J 2000 Optical transitions at the substitutional nitrogen centre in diamond *J. Phys.: Condens. Matter* **12** L77

[40] Nishikori H, Mita Y, Nisida Y, Okada M and Nakashima T 2007 Anomalous zero-phohon line broadening of the NV⁻ center in diamond *Phys. Status Solidi* c **4** 1122

[41] Zvyagin V and Manson N B 2012 Optical and spin properties of nitrogen-vacancy center in diamond crystals, nanodiamond and proximity to surfaces *Ultra-nanocrystalline Diamond: Synthesis Properties and Applications* (*Springer: Material Science and Process Technology Series*) ed O A Shenderova and D M Gruen (New York: Springer) ch 10

[42] Monticone D G, Quercioli F, Mercatelli R, Soria S, Borini S, Poli T, Vannoni M, Vittone E and Olivero P 2013 Systematic study of defect-related quenching of NV luminescence in diamond with time-correlated single-photon counting spectroscopy *Phys. Rev. B* **88** 155201

[43] Collins A T, Thomas M F and Jorge M I B 1983 Luminescence decay time of the 1.945 eV centre in 1b diamond *J. Phys. C: Solid State Phys.* **16** 2177

[44] Hanzawa H, Nisida Y and Kato T 1997 Measurement of decay time of the NV centre in 1b diamond with a picosecond laser pulse *Diam. Relat. Mater.* **6** 1595

[45] Liaugaudas G, Collins A T, Suhling K, Davies G and Heintzmann R 2009 Luminescence-lifetime mapping in diamond *J. Phys.: Condens. Matter* **21** 364210

[46] Bogdanov K V, Zhukovskaya M V, Ospov V Y, Ushakova E V, Baranov M A, Takai K, Rampersaud A and Baranov A V 2017 Highly intensive emission of the NV⁻ centers in synthetic HPHT microdiamonds at low nitrogen doping *APL Mater.* **6** 086104

[47] Biktagirov T B, Smirnov A N, Davydov V Y, Doherty M W, Alkauskas A, Gibson B C and Soltamov V A 2017 Strain broadening of the 1042 nm zero-phonon line of the NV- center in diamond: a promising spectroscopic tool for defect tomography *Phys. Rev. B* **96** 075205

[48] Dolde F *et al* 2011 Electric-field sensing using single diamond spins *Nat. Phys.* **7** 459

[49] Matsuzaki Y, Morishita H, Shimooka T, Tasima T, Kakuyanagi K, Semba K, Munro W J, Yamaguchi H, Mizuochi N and Saito S 2016 Optically detected magnetic resonance of high density ensemble of NV⁻ centers in diamond *J. Phys.: Condens. Matter* **28** 275302

[50] Forster T 1948 Intermolecular energy migration and fluorescence *Ann. Phys.* **2** 55–7

[51] Choi J *et al* 2017 Depolarization dynamics in a strongly interacting solid-state spin ensemble *Phys. Rev. Lett.* **118** 093601

[52] Jayakumar H, Henshaw J, Dhomkar S, Pagliero D, Laraoui A, Manson N B, Albu R, Doherty M W and Meriles C A 2016 Optical patterning of trapped charge in nitrogen-doped diamond *Nat. Commun.* **7** 12660

[53] Woods G S 1984 Infrared absorption studies of the annealing of irradiated diamonds *Phil. Mag.* **50** 673

[54] Stoneham A M 1966 The theory of strain broadening line shapes of spin resonance and optical zero phonon lines *Proc. Phys. Soc.* **89** 909

[55] Davies G 1970 No phonon line shapes and crystal strain fields in diamonds *J. Phys. C: Solid State Phys.* **3** 2474

[56] Davies G 1974 Vibronic spectra in diamond *J. Phys. C: Solid State Phys.* **7** 3797

[57] Rogers L J *et al* 2014 Electronic structure of negatively charged silicon-vacancy center in diamond *Phys. Rev. B* **89** 235101

[58] Pingault B, Becker J N, Schulte C H H, Arend C, Hepp C, Godde T, Tartakovskii A I, Maarkham M, Becher C and Atature M 2014 All-optical formation of coherent dark states of silicon-vacancy spins in diamond *Phys. Rev. Lett.* **113** 263601

[59] Green B L, Mottishaw S, Breeze B G, Edmonds A M, D'Haenens-Johanssson U F S, Doherty M W, Willimas S D, Twitchen D J and Newton M E 2017 Neutral silicon-vacancy center in diamond: spin polarization and lifetimes *Phys. Rev. Lett.* **119** 096402

[60] Bogdanov S *et al* 2017 Electron spin contrast of Purcell-enhanced nitrogen-vacancy ensembles in nanodiamonds *Phys. Rev. B* **96** 035146

[61] Loretz M, Takahashi H, Segawa T F, Boss J M and Degen C L 2017 Optical hyperpolarization of nitrogen donor spins in bulk diamond *Phys. Rev. B* **95** 064413

[62] Wolters J, Sadzak N, Schell A W, Schroder T and Benson O 2013 Measurement of the ultrafast spectral diffusion of the optical transition of nitrogen vacancy centers in nano-size diamond using correlation interferometry *Phys. Rev. Lett.* **110** 027401

[63] Jamonneau P *et al* 2016 Competition between electric field an magnetic field noise in the decoherence of a single spin in diamond *Phys. Rev. B* **93** 024305

[64] Bradac C, Gaebel T, Naidoo N, Sellars M J, Twamley J, Brown L J, Barnard A S, Plakhotnik T, Zvyagin A V and Rabeau J R 2010 Observation and control of blinking nitrogen-vacancy centre in discrete nanodiamonds *Nat. Nanotech. Lett.* **5** 345

[65] Inam F A, Edmonds A M, Steel M J and Casttelletto S 2013 Tracking emission rate dynamics of NV centers in nanodiamonds *Appl. Phys. Lett.* **102** 253109

[66] Ofori-Okai B K, Pezzagna S, Chang K, Loretz M, Schirhagl R, Tao Y, Moores B A, Groot-Berning K, Meijer J and Degen C L 2012 Spin properties of very shallow nitrogen vacancy defects in diamond *Phys. Rev. B* **86** 081406

[67] Liang Z Z, Jia X, Ma H A, Zang C Y, Zhu P W, Guan Q F and Kanda H 2005 Synthesis of HPHT diamond containing high concentrations of nitrogen impurities using NaN₃ as dopant in metal-carbon system *Diam. Relat. Mater.* **14** 1932–5

[68] Manson N B, Harrison J P and Sellars M J 2006 Nitrogen-vacancy center in diamond: model of the electronic structure and associated dynamics *Phys. Rev. B* **74** 104303

[69] Doherty M W, Manson N B, Delaney P and Hollenberg L C L 2011 The negatively charged nitrogen-vacancy centre in diamond: the electronic solution *New J. Phys.* **13** 025019

[70] Robledo L, Bernien H, van der Sar T and Hanson R 2010 Spin dynamics in the optical cycle of single nitrogen-vacancy centres in diamond *New J. Phys.* **13** 025013

[71] Tetienne J-P, Rondin L, Spinicelli P, Chipaux M, Debuisschert T, Roch J-F and Jacques V 2012 Magnetic-field-dependent photodynamics of single defects in diamond: an application to qualitative all-optical magnetic imaging *New J. Phys.* **14** 1030033

[72] Goldman M L, Sipahigil A, Doherty M W, Yao N Y, Bennett S D, Markham M, Twitchen D J, Manson N B, Kubanek A and Lukin M D 2015 Phonon-induced population dynamics and intersystem crossing in nitrogen-vacancy centers *Phys. Rev. Lett.* **114** 145502

[73] Lai N D, Zheng D, Jelezko F, Treussart F and Roch J-P 2009 Influence of a static magnetic field on the photoluminescence of an ensemble of nitrogen-vacancy color centers in a diamond single-crystal *Appl. Phys. Lett.* **95** 133101